Petrology and geochemistry of LaPaz Icefield 02205: A new unique low-Ti mare-basalt meteorite

Mahesh Anand [a,b,*], Lawrence A. Taylor [a], Christine Floss [c], Clive R. Neal [d], Kentaro Terada [e], Shiho Tanikawa [e]

[a] *Planetary Geosciences Institute, Department of Earth and Planetary Sciences, University of Tennessee, Knoxville, TN 37996, USA*
[b] *Department of Mineralogy, The Natural History Museum, Cromwell Road, London, SW7 5BD, UK*
[c] *Laboratory for Space Sciences, Washington University, St. Louis, MO 63130, USA*
[d] *Department of Civil Engineering and Geological Sciences, University of Notre Dame, IN 46556, USA*
[e] *Department of Earth and Planetary Sciences, Hiroshima University, Higashi-Hiroshima 739-8526, Japan*

Abstract

LaPaz Icefield 02205 (LAP 02205) is a new low-Ti mare-basalt meteorite that was discovered in the LaPaz Ice Field in Antarctica. This is the first crystalline lunar basalt in the US Antarctic collection and the only 5th unbrecciated mare-basalt meteorite to be discovered to date. The rock has a typical basaltic texture with tabular and elongated pyroxene and plagioclase crystals, and minor olivine grains commonly rimmed by pyroxenes. Core- to rim- zoning in terms of Fe and Mg is present in almost all pyroxene grains. Accessory minerals include ilmenite, chromite, ulvöspinel, troilite, and FeNi metal. This rock is highly enriched in late-stage mesostasis. Free silica is also abundant. In terms of texture and mineralogy, LAP 02205 displays features of low-Ti mare basalts, with similarities to some low-Ti Apollo 12 and Apollo 15 basalts. Whole-rock major- and trace-element compositions confirm the highly fractionated nature of this basalt. The whole-rock REE contents of the meteorite are the highest among all known low-Ti mare basalts. The platinum group element (PGE) contents in LAP are also enriched suggesting the possibility of endogenously enriched source regions or the PGEs generally behaved as incompatible elements during crystal fractionation under low fO_2 conditions. Trace-element contents of mineral grains in LAP 02205 display wide variations, suggesting extensive non-equilibrium crystallization. The REE concentrations in the earliest-formed minerals provide constraints on the composition of the parental liquid, which is similar to the measured whole-rock composition. Crystallization modeling of the LAP 02205 bulk composition yields a reasonable fit between predicted and observed mineral phases and compositions, except for the high-Mg olivine cores, which are observed in the rock but not predicted by the modeling. An isochron age of 2929 ± 150 Ma for phosphate minerals makes this rock one of the youngest lunar basalts known to date. The young age and specific geochemical characteristics of LAP distinguish it from those of most other low-Ti mare basalts. However, the low-Ti mare basalt meteorite, NWA 032, has a similar young age, and the two meteorites also appear to be closely related from some geochemical perspectives and might have originated from similar source regions on the Moon.
© 2005 Elsevier Inc. All rights reserved.

1. Introduction

The number of lunar meteorites discovered on the Earth has more than tripled in the past 10 years, mainly because of recent finds from the hot deserts of Northern Africa and the Middle East. However, there are only five unbrecciated mare-basalt meteorites found on Earth to date of which three of them come from Antarctica. Yamato-793169 (Y-793169) was the first mare-basalt meteorite from Antarctica, found in 1979, followed by Asuka-881757 (A-881757), discovered in 1988. More than a decade later, a new mare-basalt meteorite, LAP 02205 (hereafter referred to as LAP), was found in the LaPaz IceField of Antarctica during the 2002 Antarctic search for meteorites (ANSMET) field season. It was almost

* Corresponding author. Fax: +44 207 942 5537.
E-mail address: m.anand.97@cantab.net (M. Anand).

entirely covered by a fusion crust. It is the largest mare-basalt meteorite with a total weight of 1.23 kg. Subsequently, four more mare-basalt meteorites (LAP 02224, 02226, 02436, and 03632) have been discovered from the same general area and are thought to be portions of the same material from the original fall (e.g., Collins et al., 2005; Day et al., 2005). Considered together, all pieces of LAP meteorites yield a total weight of ~1.9 kg. The rock is moderately shocked, with some impact-melt veins. Terrestrial weathering features are minimal at both macroscopic and microscopic levels.

Anand et al. (2004) presented a preliminary mineralogical, textural, and geochemical description of this meteorite. This initial examination confirmed the lunar origin of LAP 02205 and its classification as a low-Ti mare basalt. The other four previously described crystalline mare-basalt meteorites (lithology A of Dhofar 287 (Dho 287A), North West Africa (NWA) 032, Y-793169, and A-881757) are also classified as low-Ti mare basalts; no crystalline basalt of high-Ti or very low-Ti variety is represented in the mare-basalt meteorite collection. This may reflect the remote-sensing observation of Giguere et al. (2000) that the majority of mare basalts are of the low-Ti variety (i.e., 1–6 wt% TiO_2, after the classification of Neal and Taylor, 1992) and that the Apollo and Luna sample collections do not reflect this. In this contribution, we present the results of our detailed mineralogical and geochemical investigations of LAP as well as U–Pb ages on phosphate grains in this meteorite. We also compare and contrast the petrological features of this sample with those of basalt samples returned by lunar missions, as well as with those of similar mare-basalt meteorites (e.g., Dho 287A and NWA 032). Finally, the possible pairing of LAP with other mare basalts is also discussed, and some inferences are drawn about the probable source regions on the Moon.

2. Analytical methods

We were allocated one thin section (LAP 02205,36), one polished thick section (LAP 02205,31), with a total area of 3.8 cm^2, and 1.572 g powdered rock sample (LAP 02205,19), by the Meteorite Working Group (MWG), for carrying out mineral and geochemical investigations.

The two polished sections of LAP were examined for textural and mineralogical characteristics. Mineral modes were determined using Feature Scan software with an Oxford Instrument Energy Dispersive Spectral (EDS) unit on an automated CAMECA SX-50 electron microprobe (EMP), following the procedure of Taylor et al. (1996). Mineral compositions were determined in wavelength dispersive spectral (WDS) mode using an accelerating potential of 15 kV, 20 nA beam current, 1 μm beam size, and standard PAP correction procedures. Counting times were 20 s for the majority of elements; however, the counting times for V and Zr were 60 and 90 s, respectively. For plagioclase analyses, a beam current of 10 nA and a beam size of >5 μm were utilized to avoid Na volatilization. Similar-

ly, a current of 10 nA and beam size of 5–10 μm were used for glass analyses.

Major-, minor-, and trace-element (including REE) concentrations were determined for selected mineral grains in LAP 02205,36 using the modified CAMECA IMS 3f ion-microprobe at Washington University, St. Louis, following the methods outlined by Zinner and Crozaz (1986a). Analyses were obtained using an O$^-$ beam with an accelerating voltage of 12.5 kV. Secondary ions were collected at low mass resolution using energy filtering (100 V offset) to remove complex molecular interferences. Simple interferences not removed by this method were corrected by deconvolution of major molecular interferences in the mass regions K–Ca–Ti, Rb–Sr–Y–Zr, and Ba–REEs (Alexander, 1994). Concentrations were obtained using sensitivity factors reported by Floss and Jolliff (1998); Hsu (1995), and Zinner and Crozaz (1986b) for the REE and by Hsu (1995) for other elements. Silicate and phosphate analyses were normalized to the reference elements, Si and Ca, respectively, using SiO_2 and CaO concentrations determined by electron microprobe.

The whole-rock, major-element compositions were determined on a 50 mg aliquot from a 1.572 g homogeneous powdered rock sample using inductively coupled plasma optical emission spectroscopy (ICP-OES) using a Perkin-Elmer Optima 3300 machine and following the method of Shafer et al. (2004). Whole-rock, trace-element measurements of LAP were also obtained on a 50 mg aliquot of powdered rock sample by solution mass spectrometry using a PlasmaQuad PQII STE machine and following the procedure of Neal (2001). Platinum group element (PGE) concentrations were determined on a 1 g rock powder using methods of Ely et al. (1999).

U–Pb age data, as well as REE contents, of phosphate grains in LAP were measured with an ion-microprobe (SHRIMP) at Hiroshima University, Japan, using the method described in Terada and Sano (2004).

3. Petrography and mineral chemistry

Lunar meteorite LAP 02205 is a coarse-grained, holocrystalline basalt consisting mainly of crystals of pyroxene and plagioclase (both up to 2 mm) with some minor high-Mg olivine (Figs. 1A and B). Laths of ilmenite, up to 1 mm long, are distributed throughout the sample and constitute the major portion of the oxide minerals, which also includes chromite and ulvöspinel. Troilite and FeNi metal occur in minor amounts. The rock is apparently not as strongly shocked as other basaltic lunar meteorites such as Dho 287A and NWA 032. Shock features include only partial maskelynitization of plagioclase, planar deformation features in some pyroxenes, presence of few melt veins (Fig. 1C), and step-type fractures in ilmenite grains (Figs. 1A, D, and F). A conspicuous feature of the rock is the abundance of mesostasis, similar to that seen in Dho 287A (Figs. 1E and F) (Anand et al., 2003a). Free silica occurs throughout the two polished sections that we have
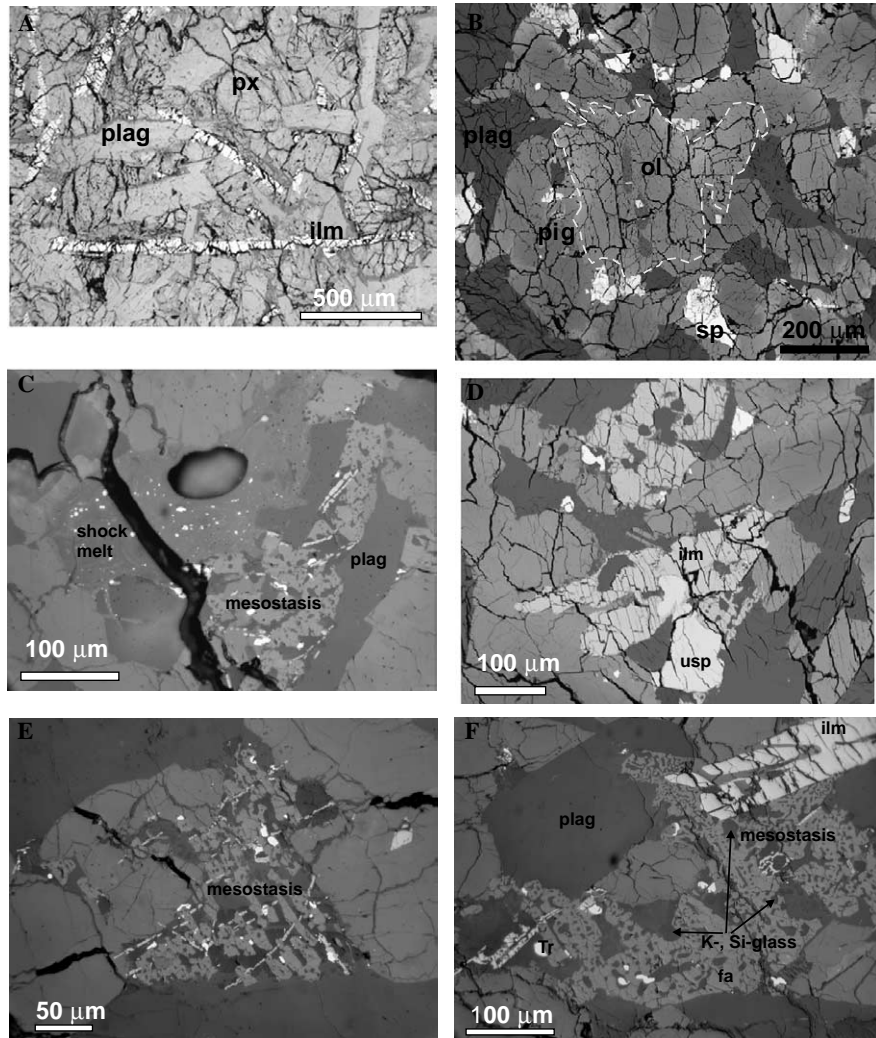
Fig. 1. Photomicrographs illustrating textures and mineralogy of LAP 02205. (A) Reflected-light image showing the coarse-grained, holocrystalline texture of the rock, which is defined by euhedral to subhedral grains of plagioclase (plag), pyroxene (px), and ilmenite (ilm). (B) Back-scatter electron (BSE) image of an area illustrating rimming of olivine (ol) by pyroxene (px). The subtle contrast in the gray is marked by the dashed line, which follows the olivine–pyroxene contact. (C) Reflected-light view of an area of the thin section showing a small pool of shock-induced melt veins. Specks of troilite are seen distributed throughout this melt. A small mesostasis area is also present near the bottom right of the image. (D) BSE image showing intergrown ulvöspinel (usp) and ilmenite (ilm) grains. (E and F) Reflected-light view of mesostasis areas illustrating typical "swiss cheese" texture. The light-gray areas are composed of fayalite (fa) and dark areas are K–Si-rich glass, sometimes crisscrossed by small ilmenite laths and surrounded by large grains of Fe-pyroxenes. Brighter spots are troilite grains.

examined, although not always associated with the mesostasis areas. Collins et al. (2005) have reported that Raman spectroscopic measurements confirmed this silica phase to be cristobalite.

The modal mineralogy of LAP, as measured on two polished sections using the X-ray digital-imaging procedure of Taylor et al. (1996), is given in Table 1. This technique is an automated point counting technique utilizing an EMP in which an Energy Dispersive X-ray spectrum is collected at each point. This spectrum is then classified as a mineral based on the percentage of total counts of diagnostic elements for that mineral. Appropriate boundary conditions are used to distinguish various minerals. For example, plagioclase is distinguished from pyroxene based upon Al con-

tent, and from spinel, based upon Si content. Similarly, different types of pyroxenes, i.e, pigeonite, augite, and ferropyroxene, are distinguished based upon a combination of various elemental intensities such as Ca, Mg, and Fe contents. Boundary conditions used for pyroxenes in the present case were: pigeonite (Si 42–76%, Ca 4–12%, and Mg 2–22%), augite (Si 42–72%, Ca 12–35%, and Mg 2–22%), and ferropyroxene (Si 40–70%, Ca 5–35%, Mg 0–2%, and Fe 19–55%). The ranges of elements have been determined from numerous quantitative analysis results, used to characterize this sample.

Table 1 also lists data for other mare-basalt meteorites, and some Apollo 12 and Apollo 15 low-Ti mare basalts for comparison. The X-ray elemental maps (Figs. 2A–D) of

Table 1
Modal abundances (vol %) in low-Ti lunar mare-basalt meteorites and similar lunar basalts from Apollo 12 and 15

	Mare-basalt meteorites						Apollo 12 and 15 basalts		
	LAP 02205	Dho 287A	NWA 032	Y-793169	A-881757	EET 87521 (clast A)	12016,25	12054	15556,136
	1	2	3	4	5	6	7	7	8
Olivine phenocrysts	1.2	20.6	11.3	0	0	15	12	10.8	0.1
Chromite phenocrysts	0.1	0.4	0.3	0	<5	—	0	1.9	0.4
Pigeonite	12.0	29.3	—	—	—	—	—	—	—
Augite	29.0	15.7	—	—	—	—	—	—	—
Fe–pyroxene	15.9	2.4	—	—	—	—	—	—	—
Undifferentiated pyroxene	56.9	47.4	50.7	56	59	44	52.1	62.1	57
Feldspar/maskelynite	33.1	25.9	29.4	42	30	39	29.1	27.9	38
Ilmenite	3.3	2.3	4.4	1	6	2	4.8	5.2	2.1
Ulvöspinel	0.4	0.83	tr	1	<5	0	1.6	0.5	0.6
Troilite	0.2	0.1	0.7	0	<5	0	0	0.3	0.1
FeNi metal	tr	tr	tr	0	<5	0	0	0.1	tr
Opaque minerals (total)	4.0	3.63	5.4	2	<11	2	6.4	8	3.2
Silica	2.3	0.2	0	0	0	0	0	0.1	0.8
Phosphate	0.3	0.6	—	—	—	—	—	—	—
Fayalite	1.5	0.2	—	—	—	—	—	—	—
Melt glass	0.8	1.4	3.2	0	0	0	0	0	0
Mesostasis	>4	>3	0	0	0	0	0.6	1.9	1

Data sources: 1, Anand et al. (2004); 2, Anand et al. (2003a); 3, Fagan et al. (2002); 4, Takeda et al. (1993); 5, Yanai and Kojima (1991); 6, Warren and Kallemeyn (1989); 7, Neal et al. (1994); 8, Rhodes and Hubbard (1973).

the polished sections also help to bring out the overall mineralogical and textural makeup of the rock. For example, the Mg X-ray map (Fig. 2A) assisted in locating the Mg-rich olivine and pyroxene grains. Similarly, the relatively homogeneous distribution of cristobalite became apparent from the Si X-ray map (Fig. 2B). Overall, we feel confident that a representative portion of the rock has been analyzed.

A distinctive petrographic feature of LAP is the unusual abundance (>3%) of late-stage mesostasis, composed mainly of symplectic intergrowth of fayalite and Si–K-rich glass. Fluor-apatite and whitlockite grains, as well as ilmenite and Fe metal, also occur in these areas. The mesostasis areas, common to many lunar basalts, show the typical "swiss cheese" pattern that is easily identifiable in reflected light (Figs. 1E and F). These areas are identical to those described from Dho 287A (Anand et al., 2003a). As in Dho 287A, we believe that these mesostasis areas are the result of silicate-liquid immiscibility (SLI) that occurs after >95% melt crystallization. The occurrence of SLI in lunar basalts has been discussed in great detail by a number of authors (e.g., Rutherford et al., 1974; Hess et al., 1978; Neal and Taylor, 1989, 1991), and this feature has been used as an indicator of highly fractionated basalts.

Based on texture and mineralogy, LAP appears to be similar to low-Ti Apollo 12 and 15 basalts (hereafter referred to as A 12 and A 15, respectively), but is more akin to A 12 pigeonite and A 15 quartz normative basalts (Vetter et al., 1987). However, as discussed below, this rock has other unique geochemical characteristics, which do not match with those of any single known mare basalt, thus, suggesting that LAP may be a new variant of lunar basalt. In the following sub-sections, a detailed mineralogy of the rock is provided.

3.1. Silicate mineralogy

There are a few high-Mg olivine grains (Fo 60 and higher) in LAP 02205, which occur as large crystals (up to 0.5 mm), most with moderate chemical zonation. They commonly have skeletal habit and are overgrown by pigeonite (Fig. 1B), which also shows chemical zonation. This textural feature suggests a reaction relationship between olivines and pyroxenes. The preservation of Fe–Mg zoning in olivine grains also suggests that even if these grains are xenocrystic, they must have formed not long before the onset of crystallization of the LAP magma. One possibility is that the olivine grains might have been derived by fractionation of a slightly more magnesian magma immediately preceding LAP eruption through the same magma chamber. The fayalitic olivines (Fo 15 or less) are exclusively restricted to mesostasis areas where they occur with Si–K–glass and probably formed during the last stages of magma crystallization. Electron microprobe data for a number of olivine grains were collected to obtain the range of Fo contents (Fig. 3). Representative compositions of the mineral phases present in LAP are listed in Table 2. The similarity in the range of olivine compositions in LAP to those of A 12, and A 15 low-Ti basalts, and to those of Dho 287A is also evident (Fig. 3C). Lunar meteorite NWA 032 lacks fayalitic olivines, also consistent with the absence of mesostasis in this rock (Anand et al., 2003b), presumably due to rapid cooling of the extruded magma, which led to the development of plumose groundmass texture as described by Fagan et al. (2002). Since LAP is mineralogically and texturally similar to low-Ti mare basalts, it is mainly compared and contrasted with low-Ti mare basalt samples in subsequent sections.
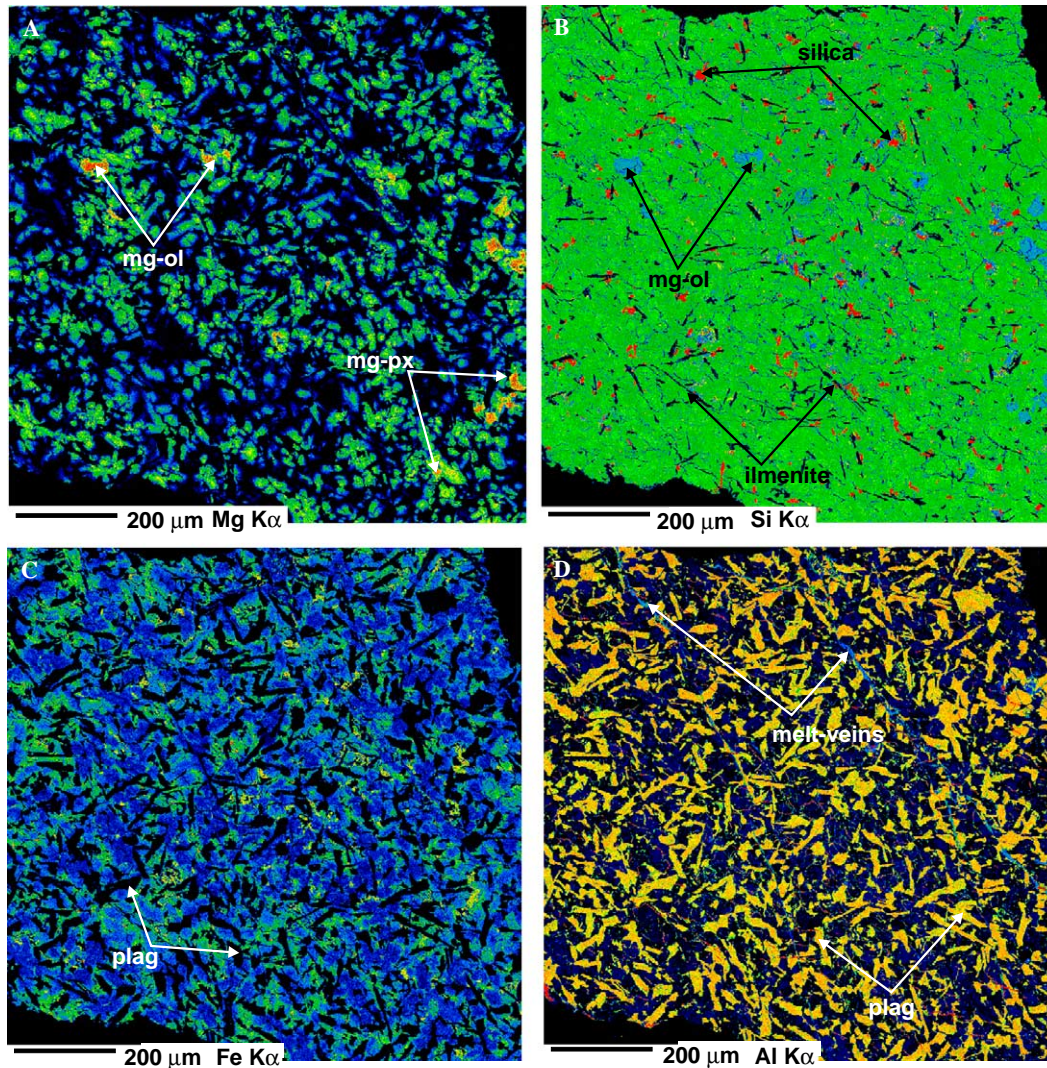
Fig. 2. X-ray elemental maps of LAP 02205. Brighter shades correspond to higher intensity. (A) Mg X-ray map; cores of early formed pigeonites and olivines appear orange. (B) Si X-ray map; free silica (red); Ilmenite laths are black and Mg-rich pyroxenes and olivines are in cyan. (C) Fe X-ray map; plagioclase (plag) laths are highlighted in black. (D) Al X-ray map; plagioclase laths are in bright yellow. Two melt-veins are seen in cyan that seem to run parallel across the thin section.

Pyroxene is the most abundant mineral in LAP and occurs as coarse-grained, tabular crystals. Some of the pyroxene grains display lamellar features in cross-polarized light that initially appear to be exsolution lamellae. However, EMP analyses did not show any chemical differences between the host and the lamellae, and thus, these are ascribed to shock-induced twinning. Pyroxene compositions exhibit extreme variations (Fig. 3A) and follow the commonly observed fractionation trends in mare basalts (e.g., Papike et al., 1976). Like the olivines, pyroxenes in LAP also display 'normal' zoning but show a larger degree of Fe-enrichment in their outer portions. The late-stage ferropyroxenes occur as ferroaugite and ferropigeonite. Some ferropyroxenes have compositions of pyroxferroite (Fig. 3A).

During the crystallization of a basaltic magma, the Al to Ti ratios in pyroxene varies depending upon appearance and disappearance of other liquidus phases. For example, plagioclase on the liquidus affects the amount of Al uptake into the pyroxene structure. Similarly, ilmenite crystallization affects Ti uptake in pyroxene. Furthermore, high Ca pyroxene accommodates larger amounts of Al and Ti compared to low-Ca pyroxene. Al to Ti ratio in pyroxenes also vary systematically with their Mg# (Mg/Mg + Fe) with progressive fractionation. Thus, the co-variation between Al and Ti, and, Al/Ti and Mg# in pyroxenes may provide useful information about crystallization sequence of a magma. Al to Ti ratios in high-Mg LAP pyroxenes vary from 4:1 to ∼3:1 (Fig. 4A), consistent with pyroxene being the first-formed mineral in the rock. However, this ratio decreases gradually with decreasing Mg#, suggesting the appearance of plagioclase on the liquidus (at around Mg# 55; Fig. 4B). This led to Al depletion in the residual melt with concomitant increase in the Ti content, causing
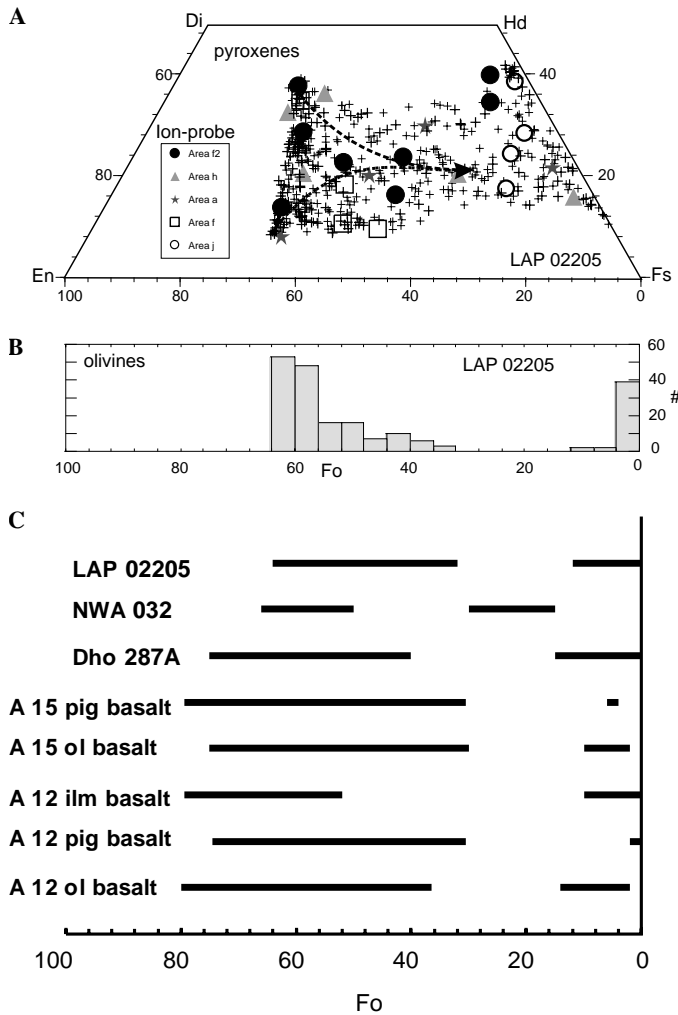
Fig. 3. Compositional variation of pyroxenes and olivines in LAP 02205. (A) Pyroxene compositions range from high-Mg augite and pigeonite to ferroaugite and pyroxferroite. (B) Histogram shows the bimodal distribution of Fo contents in olivine grains. (C) Comparison of olivine Fo contents in LAP with those of other low-Ti mare basalts. Modified after Anand et al. (2003a).

an eventual decrease in Al to Ti ratio. At around Mg#40, ilmenite joined pyroxene and plagioclase on the liquidus, reducing the Ti content of the residual magma. Subsequently, the Al to Ti ratio remained constant at around 1.5 as all three phases crystallized together untill the end. The Al and Ti contents along a traverse across one pyroxene grain are plotted in Fig. 4A, showing similar variations as described above. The general sequence of appearance of major phases deduced from the Al and Ti variations in pyroxenes is also consistent with the results of crystallization modeling discussed in a later section.

Plagioclase in LAP occurs as tabular crystals and is only partially converted into maskelynite; in most cases, even the original twinning is preserved. Plagioclase compositions also follow the typical fractionation trend for mare basalts. The An contents vary from 84 to 90 (Fig. 5), similar in range to that of low-Ti mare basalts such as those

from the A 12 and A 15 collections, albeit slightly Na-enriched. Cooling-rate estimates, based on the thickness of plagioclase laths (Grove and Walker, 1977), yield values of 0.2–0.8 °C/h for the lava, typical for the center of a 10–20 m thick flow.

3.2. Opaque mineralogy

Opaque minerals are abundant (i.e., ~3–4%) throughout the LAP basalt. Ilmenite is the most abundant, occurring as lath-shaped grains (Fig. 1), and in some cases, shows a lamellar structure, indicative of shock (Taylor et al., 1971). Ilmenite compositions are almost pure $FeTiO_3$, with the majority of them having no significant geikielite ($MgTiO_3$) (<0.1 wt% MgO) or pyrophanite ($MnTiO_3$) (<0.5 wt % MnO) components.

Spinels are the second most abundant of the opaque minerals and occur as aluminous chromite rimmed by ulvöspinel, with the latter being more abundant. Cr-rich spinel generally occurs in or near forsteritic olivine. The LAP spinel compositions follow fractionation trends similar to spinels in A 12 and A 15 mare basalts (Figs. 6A and B) (Taylor et al., 1971; El Goresy, 1976). The boundary between chromite and ulvöspinel appears to be sharp and intermediate compositions are probably due to "edge-effects." There is evidence for sub-solidus reduction of ulvöspinel to ilmenite + Fe metal, as commonly seen in mare basalts (e.g., Taylor et al., 1971). In some instances, ilmenite and spinel are in direct contact with each other (Fig. 1D). However, the ZrO_2 content across the grain boundaries varies non-systematically, preventing a precise cooling rate estimation based on Zr partitioning data (Taylor et al., 1975). The reason for this non-systematic variation in ZrO_2 content is not clear but we suspect that the shock event that launched this meteorite from the Moon may be responsible. Troilite (FeS) and FeNi metal also occur, albeit sparsely distributed. These are exclusively associated with later-formed minerals in the mesostasis areas, in pyroxenes or at grain boundaries of pyroxenes and plagioclases. This is in contrast with Apollo 12 basalts where FeNi metal grains are associated with the earliest-formed minerals such as chromite and olivine. In the LAP 02205 basalt, the Ni and Co contents in FeNi metals vary over a significant range (5.3–16 wt% Ni; 1.3–3.4 wt% Co). Studies of other pairs of LAP basalts have confirmed the occurrence of even larger ranges in Co and Ni contents (0.85–5.6 wt% Co and 0.3–30 wt%) in metal grains (Schnare et al., 2005); in one metal grain in LAP 02226, the Ni content is reported to be as high as 61.4 wt% (Taylor and Day, 2005). Such high concentrations of Co and Ni in apparently later-formed metal grains have been interpreted to be due to lack of significant crystallization of olivine and chromite at the earliest stages of magma crystallization, which would otherwise deplete the residual magma in these elements. Another possible explanation for the elevated Co and Ni contents in LAP metal grains is meteoritic contamination. However, this can be ruled out based on the Ni–Co

Table 2
Representative electron microprobe analyses (wt %) of constituent minerals in LAP 02205

Phases	Mg-Pig.	Mg-Aug.	Fe-Px	Olivine	Fayalite	Plagioclase	K-glass	Si-glass	Apatite	Ilmenite	Chromite	Ulvöspinel
SiO_2	52.2	50.0	45.8	36.2	29.3	47.5	74.1	99.0	1.5	0.03	0.06	0.07
TiO_2	0.44	1.22	0.87	0.03	0.40	na	na	na	na	52.0	5.24	28.9
Al_2O_3	0.89	2.86	0.85	0.04	<0.03	32.1	11.1	0.34	na	0.11	11.9	4.62
Cr_2O_3	0.54	0.93	<0.03	0.15	<0.03	na	na	na	na	0.07	43.9	7.79
MgO	20.2	15.2	0.93	30.6	0.38	0.33	<0.03	<0.03	<0.03	0.11	3.60	2.10
CaO	5.13	12.9	11.5	0.37	0.91	17.5	0.65	0.08	51.7	0.03	0.03	0.17
MnO	0.39	0.33	0.52	0.36	0.65	na	na	na	na	0.29	0.24	0.34
FeO	20.6	16.4	38.8	32.8	67.6	0.68	2.15	0.12	1.93	46.5	33.3	55.1
Na_2O	<0.03	0.04	<0.03	na	na	1.32	0.08	0.07	0.01	na	na	na
K_2O	na	na	na	na	na	0.03	7.87	0.08	na	na	na	na
P_2O_5	na	na	na	na	na	na	na	na	39.4	na	na	na
ZrO_2	na	na	na	na	na	na	na	na	na	0.06	na	0.15
V_2O_3	na	na	na	na	na	na	na		na	na	0.78	0.29
Cl	na	na	na	na	na	na	na	na	0.55	na	na	na
F	na	na	na	na	na	na	na	na	1.86	na	na	na
Total	100.4	99.9	99.3	100.6	99.2	99.4	96.0[a]	99.7	96.0	99.2	99.1	99.3
Based on	6 O	6 O	6 O	4 O	4 O	8 O			24 O	3 O	4 O	4 O
Si	1.951	1.892	1.948	0.989	0.994	2.199			0.240	—	0.002	0.003
Ti	0.012	0.035	0.028	—	—	—			—	0.995	0.137	0.782
Al	0.039	0.127	0.043	—	—	1.751			—	0.003	0.486	0.196
Cr	0.016	0.028	0.001	—	—	—			—	0.001	1.202	0.222
Mg	1.128	0.86	0.059	1.245	0.019	0.023			—	0.004	0.186	0.113
Ca	0.206	0.523	0.524	0.011	0.033	0.867			9.041	0.001	0.001	0.007
Mn	0.012	0.011	0.019	0.008	0.019	—			—	0.006	0.007	0.01
Fe	0.643	0.518	1.381	0.749	1.919	0.026			0.264	0.988	0.964	1.661
Na	—	0.003	0.001	—	—	0.119			0.003	—		
K	—	—	—	—	—	0.002			—	—		—
P	—	—	—	—	—	—			5.443	—	—	—
Zr	—	—	—	—	—	—			—	0.001	—	—
V	—	—	—	—	—	—			—	—	0.022	0.008
Total	4.01	4.00	4.00	3.01	3.00	4.99			15.0	2.00	3.01	3.00
Mg#	63.7	62.4	4.10	62.4	0.98	—				—	—	—
Fe#	36.3	37.6	95.9	37.6	99.0	—			—	—	—	—
An#	—	—	—	—	—	87.8			—	—	—	—
Cr#	—	—	—	—	—	—			—	—	65.9	18.5

Mg-Pig., Mg-pigeonite; Mg-Aug., Mg-augite; Fe-Px, pyroxferroite; na, not analyzed.

[a] Difficulty in getting good analyses due to very small grain size.

trend in LAP basalts, which plots away from the 'typical' iron, chondrite, or achondrite fields (Taylor and Day, 2005). Moreover, a Re–Os study has not revealed any evidence for an 'exogenous' meteoritic components in LAP basalts (Day et al., 2005).

4. Petrogenesis

4.1. Whole-rock geochemistry

The selected whole rock, major, trace, and rare-earth-element data for LAP 02205, and other similar mare basalts, are presented in Table 3. Compared to other low-Ti lunar basalts, the MgO content in LAP is at the lower end whereas SiO_2 and Al_2O_3 contents are relatively enriched. In addition, this rock has relatively high abundances of Na_2O, K_2O, and other incompatible elements. The Mg# of the rock is ~31, similar to some A 15

quartz-normative basalts (QNBs). However, at the same Mg#, LAP is more enriched in incompatible trace elements than any known A 12 or A 15 QNB sample (Table 3). This feature strongly points to a distinct petrogenetic history for LAP.

Based on the classification scheme of Neal and Taylor (1992) for lunar basalts, LAP 02205 can be classified as a low-Ti mare basalt (Fig. 7A). In Fig. 7, data for mare basalts, returned from both Apollo and Luna missions (compiled from various sources), as well as data for some of the mare-basalt meteorites, are shown for comparison. LAP basalt is depleted in MgO content compared to most low-Ti mare basalts. However, the Y-793169 and A-881757 basaltic meteorites have MgO and TiO_2 contents comparable to those of LAP but as shown later, they differ significantly in terms of other major and trace element signatures. In terms of other major elements, LAP is enriched in Al_2O_3 and CaO content, compared to A 12 and A 15 low-Ti
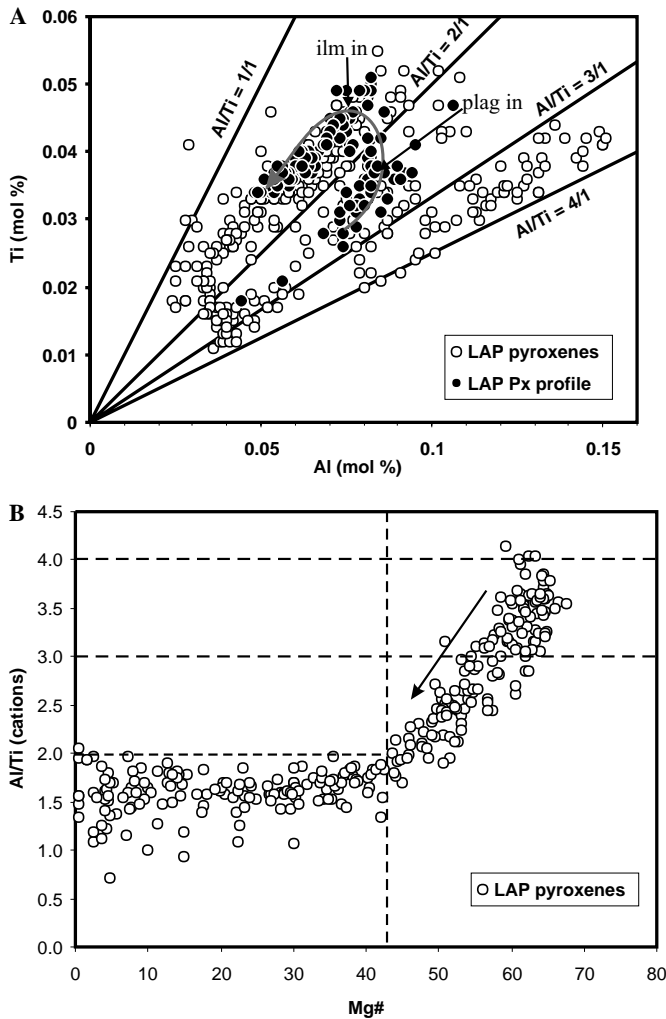
Fig. 4. (A) Plot of Al (mol %) vs. Ti (mol %) in LAP pyroxenes. The solid black symbols are data points collected along a traverse across a pyroxene grain. The gray arrow indicates the general trend in Al and Ti variation with increasing crystallization. "plag in" and "ilm in" mark inflexion points when plagioclase and ilmenite appeared on the liquidus, respectively. (B) Mg# vs. Al/Ti ratios in LAP pyroxenes.
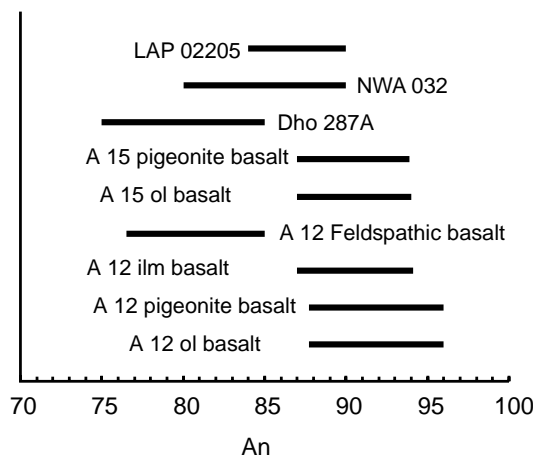

Fig. 5. Comparison of plagioclase An contents in LAP with those of other low-Ti mare basalts, modified after Anand et al. (2003a).

mare-basalts (Fig. 7B; Table 3), indicative of the fractionated nature of the LAP basalt. These observations are consistent with the textural and mineralogic data that confirm the low modal olivine content in the rock, as well as the presence of Fe-enriched mineral phases and the high-modal plagioclase content of the rock.

The bulk-rock, trace, and REE chemistry further highlights the incompatible trace-element-enriched nature of LAP 02205. In a plot of $(La/Yb)_n$ vs. $(Sm)_n$ (Fig. 8A), it is evident that LAP is LREE-enriched with a similar $(La/Yb)_n$ ratio to that of some low-Ti mare basalts, especially to that of lunar meteorite NWA 032. A prominent negative Eu anomaly (i.e., $(Sm/Eu)_n > 1$), characteristic of all mare basalts, and the LREE-enriched nature are indicated by a plot of chondrite-normalized $(La)_n$ vs. $(Sm/Eu)_n$ (Fig. 8B).

LAP has the highest chondrite-normalized abundances of REEs among mare-basaltic meteorites and low-Ti basalts from Apollo and Luna sample return missions (Fig. 9). Some of the mare-basalt meteorites and A 12 and A 15 mare basalts show positive slopes in their LREE patterns, compared to the negative slope shown by LAP. The LREE-enriched nature of LAP cannot easily be ascribed to the effects of terrestrial weathering (Crozaz et al., 2003), since there is no petrographic evidence for significant terrestrial alteration in the sample. The LREE-enriched nature of LAP basalt is, therefore, more reflective of an LREE-enriched source region. Ion-microprobe study of individual minerals provides further support for this interpretation. Weathering of Antarctic meteorites often results in the presence of Ce anomalies in individual minerals (e.g., Floss and Crozaz, 1991). We note that no Ce anomalies were observed in any of the mineral analyses of LAP.

The platinum group element (PGE) contents of the Moon are considered to be depleted relative to the Earth (e.g., Righter et al., 2000). This interpretation is based mainly on iridium contents of lunar rocks as measured by radiochemical neutron activation analysis. However, the database is not robust because only small and limited numbers of lunar samples have been analyzed, increasing the likelihood of accentuating the nugget effect associated with PGE distributions in silicate rocks. For example, there is a wealth of published experimental work that show PGE solubility in silicate melts is a function of oxygen fugacity (fO_2), with increasing fO_2 resulting in increased PGE solubility (e.g., Amossé and Allibert, 1993; Borisov et al., 1994; Borisov and Palme, 1995, 1997; Borisov and Nachtweyth, 1998; Borisov and Walker, 2000; Walter et al., 2000). Below fO_2 of approximately 10^{-5} bars, zerovalent PGE species occur and nugget effects are also most notable (e.g., Borisov and Palme, 1998; Ertel et al., 1999). The crystallization of mare basalts occurred just below the iron-wüstite buffer at an oxygen fugacity of $\sim 10^{-14}$ bars (Sato, 1976; Sato et al., 1973; Tuthill and Sato, 1970), well within the conditions where the PGE nugget effect would occur. Therefore, the analyses of Ir by radiochemical neutron activation reported during the 1970s that showed different aliquots of the same sample yielding radically different
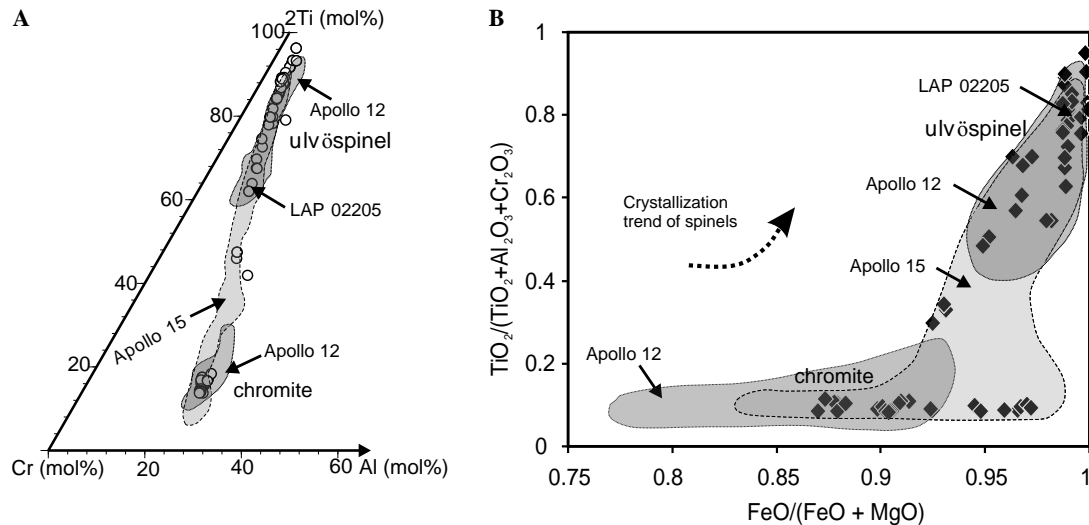
Fig. 6. (A) Spinel analyses plotted on a ternary plot of 2Ti–Cr–Al (in mol %). Spinel compositions follow the lunar trend defined by Apollo 12 and 15 samples. (B) Plot of FeO/(FeO + MgO) vs. $TiO_2/(TiO_2 + Cr_2O_3 + Al_2O_3)$ (in wt %) for LAP 02205 spinels also shows a crystallization trend similar to those defined by A 12 and A 15 spinels (data from El Goresy, 1976).

concentrations probably reflect the heterogeneous distribution of the PGEs in the low-fO$_2$ mare basalts; the "high" concentrations are not due to contamination during handling and/or processing (e.g., Anders et al., 1971; Baedecker et al., 1971). As such, Neal et al. (2001) concluded that pristine lunar samples could contain Ir abundances that exceed 1 ng/g. This is the reason why we, unlike previous work, used over 1.5 g of homogenized material in an attempt to minimize the nugget effect.

It is possible that elevated PGE abundances in lunar samples are because of meteoritic contamination. There have been several studies that have endeavored to classify the meteorite impactor and also the indigenous lunar siderophile element budget (e.g., Delano and Ringwood, 1978; Righter et al., 2000). Development of new methods has allowed precise measurements of a large suite of PGEs (Ir, Ru, Rh, Pt, and Pd). Similar geochemical behavior among these highly siderophile elements allows a more rigorous assessment of 'endogenous' vs. 'exogenous' source contributions in a manner similar to that of chondrite-normalized REE plots in igneous geochemistry. Neal et al. (2001) showed that on a chondrite-normalized plot, pristine lunar basalts display a smooth pattern with increasing abundance from Ir to Pt. Samples that contain an 'extraneous' component, however, deviate from this trend, resulting in a flatter normalized PGE pattern. The PGE abundances in LAP basalt are the highest values measured in any lunar basalt to date (Table 4). Based on the previous classification schemes, a significant amount of meteoritic contamination would be needed to explain this feature. However, on a chondrite-normalized plot, the PGE pattern for LAP basalt shows a smooth pattern with increasing abundance from Ir to Pt, comparable to that of chemically pristine low-Ti mare basalt 12001,826, albeit with much higher absolute abundances (Fig. 10). Also, the lunar basaltic

meteorite, EET 96008, has a PGE pattern similar to that of LAP. The platinum abundance in LAP basalt, however, is close to some of the highest values seen in the impact melt breccias reported by Norman et al. (2002) but other elements are generally lower (Fig. 10). Thus, the PGE signature could indicate that LAP 02205 is a new variant of low-Ti lunar basalt, which was probably derived not only from an incompatible-element-enriched source, but also from an endogenously enriched PGE source, on the Moon. This observation is also consistent with the Re–Os isotopic study of LAP 02205 by Day et al. (2005), which gave no credence to the presence of an 'exogenous' meteoritic component in that basalt. Alternatively, this could indicate that the PGEs generally behaved incompatibly during crystal fractionation under low fO$_2$ conditions and this accounts for their relative overall enrichment.

4.2. Trace-element variations in minerals and petrogenetic modeling

Based on the large variation observed in terms of major elements in LAP pyroxenes, we investigated the trace-element compositions of a number of pyroxene grains whose compositions plot in different parts of the pyroxene quadrilateral (Fig. 3). We also selected several grains of plagioclase, olivine, and phosphate minerals for trace-element analysis to assess the level and extent of variations preserved in them. Using mineral REE data and appropriate partition coefficients, REE contents of the parental melts in equilibrium with the earliest-formed phases have also been calculated. The complete ion-microprobe REE dataset is listed in Table 5.

The REE abundances in LAP pyroxenes display significant variations on a chondrite-normalized plot (Fig. 11A), suggesting an extensive fractional-crystallization history of

Table 3
Major and trace-element compositions of lunar mare-basalt meteorites and similar basalts from Apollo 12 and 15 collections

	Mare basalt meteorites						Apollo 12 and 15 basalts								
	LAP 02 205	Dho 287A	NWA 032	Y-793169	A-881757	EET 87521 (clast A)	12016,9	12054,62	15119,19	15556,177	A 12 QNB 12,056	A 12 QNB 12,047	A 15 QNB B-22	A 15 QNB B-45	15,475,152
wt %		1	2	3	3	4	5	5	6	6	7	7	8	8	9
SiO$_2$	45.2	43.2	44.7	46.0	47.1	48.4	42.8	45.9	44.9	45.7	43.4	45.1	47.5	46.9	49.0
TiO$_2$	3.38	2.76	3.08	2.19	2.45	1.13	4.02	4.63	2.57	2.62	5.07	5.20	2.49	2.63	1.75
Al$_2$O$_3$	10.0	8.35	8.74	11.1	10.0	12.5	7.23	10.5	8.96	9.48	8.82	10.10	13.00	12.71	9.77
Cr$_2$O$_3$	0.19	0.65	0.40	0.24	0.29	0.21	0.57	0.33	0.59	0.84	0.48	0.31	0.16	0.16	0.36
FeO	23.2	22.1	23.0	21.2	22.5	19.2	22.6	19.5	22.2	21.7	21.6	20.5	19.7	21.0	19.9
MnO	0.23	0.29	0.33	0.32	0.34	0.24	0.30	0.29	0.28	0.28	0.29	0.29	0.22	0.26	
MgO	5.99	13.2	8.45	5.75	6.30	6.30	12.7	6.76	9.38	8.15	9.30	6.59	4.61	4.92	8.42
CaO	11.2	8.74	10.9	12.0	11.8	11.7	8.42	11.9	10.0	10.6	10.2	11.3	11.5	11.6	10.8
Na$_2$O	0.33	0.53	0.37	0.27	0.25	0.41	0.22	0.31	0.26	0.26	0.29	0.31	0.31	0.27	0.31
K$_2$O	0.11	0.19	0.11	0.06	0.04	0.07	0.06	0.07	0.05	0.05	0.07	0.08	0.04	0.05	0.05
P$_2$O$_5$	0.12	0.21	—	—	—	0.08	0.06	0.07	0.07	0.07	0.08	0.10	0.06	0.05	
Total	100.0	100.2	99.7	99.2	101.0	100.0	99.0	100.2	99.2	99.6	99.6	99.9	99.6	100.5	100.4
Mg#	31.4	51.5	39.6	32.6	33.3	37.3	49.9	38.2	43.0	40.1	43.33	36.34	29.39	29.38	42.90
	ppm	µg/g	µg/g	µg/g	µg/g	µg/g	µg/g	µg/g	µg/g	µg/g					
Li	11.70	—	—	—	—	—	—	—	—	—					
Be	1.37	—	—	—	—	—									
Sc	58.6	35.2	56	93.7	99.4	44	—	—	44	46	60	61			
V	129.0	—	—	—	—	—	—	—	—	—					
Co	37.3	42.3	42	29.8	27.9	46	54	31	50	50	42	32			
Ni	27.6	20	50	53	52	29	25	—	59	63					
Rb	2.1	—	—	—	—	—	—	—	—	—					
Sr	135.3	530	142	78	115	104	126	162	112	101	159	171			
Y	73.2	—	—	—	—	—	—	—	—	—	55	57			
Zr	200.3	60	175	59	45	140	117	128	95	94	135	141			
Nb	14.7	—	—	—	—	—	—	—	—	—	6	7			
Cs	0.1	—	—	—	—	—	—	—	—	—					
Ba	164.7	200	242	34	27	88	59	64	44	44	62	69			
La	13.40	12.9	11.2	4.72	3.69	8.3	—	—	5.36	5			7	8	5
Ce	37.31	30.3	29.7	14.8	10.9	20.9	16.2	18.8	15.9	15.8	20.2	20.1	21.1	22.5	15.0
Pr	5.15	—	—	—	—	—	—	—	—	—					
Nd	25.12	20.4	21	11.9	8.31	13	—	—	15	13			17	22	11
Sm	7.56	6.31	6.61	4.3	2.88	3.86	5.5	6	3.82	3.65	6.40	6.50	4.55	4.77	3.45
Eu	1.24	1.18	1.1	1.31	1.1	0.98	1.06	1.27	0.94	0.96	1.31	1.36	0.98	1.00	0.92
Gd	9.95	—	—	—	—	—	—	—	—	—					
Tb	1.93	1.22	1.56	1.02	0.76	0.8	1.42	1.85	0.83	0.87	1.73	1.80	0.99	1.11	0.79
Dy	12.08	—	—	—	—	—	—	—	—	—					
Ho	2.45	—	—	—	—	—	—	—	—	—					
Er	6.71	—	—	—	—	—	—	—	—	—					
Tm	0.94	—	—	—	—	—	—	—	—	—					
Yb	6.37	3.35	5.79	4.59	3.26	3.19	5	5.8	2.36	2.27	6.00	5.90	3.08	3.29	2.45
Lu	0.88	0.51	0.8	0.66	0.52	0.48	0.67	0.78	0.32	0.31	0.82	0.89	0.47	0.48	0.38
Hf	5.39	2.64	5	3.01	2.2	2.88	6.3	4.8	2.89	2.89	4.80	5.10			
Ta	0.77	0.71	0.62	0.31	0.22	0.37	—	—	0.41	0.39					
W	0.20	—	—	—	—	—	—	—	—	—					
Pb	1.00	—	—	—	—	—	—	—	—	—					
U	0.55	—	—	—	—	—	—	—	—	—					
Th	2.33	0.9	1.9	0.68	0.42	0.95	—	—	0.49	0.46			0.87	1.01	

Data sources: 1, Anand et al. (2003a); 2, Fagan et al. (2002); 3, major elements from Warren and Kallemeyn (1993) and minor elements from Koeberl et al. (1993); 4, Warren and Kallemeyn (1989); 5, Rhodes et al. (1977); 6, Ryder and Schuraytz (2001); 7, Rhodes et al. (1977); 8, Vetter et al. (1987); 9, Ryder (1985).

the LAP magma. Most pyroxenes have sub-parallel convex upward patterns, which are HREE-enriched with deep negative Eu anomalies. Pyroxenes with high-Mg cores have REE abundances lower than those in Fe-rich rims. The slope of the LREE pattern also becomes less steep with progressive fractional crystallization. The co-variation of (La/Yb)$_n$ values with the Wo and En contents of pyroxenes

is illustrated in Figs. 11B and C, respectively. In general, the (La/Yb)$_n$ values in pigeonite are lower than those in augite or sub-calcic augite owing to the higher affinity of LREEs in the high-Ca pyroxene structure. Also, (La/Yb)$_n$ increases with an increasing degree of fractionation. Three pyroxene grains (f2px40, jpx71, and hpx 64; Table 5) are distinctly more LREE-enriched, such that the overall
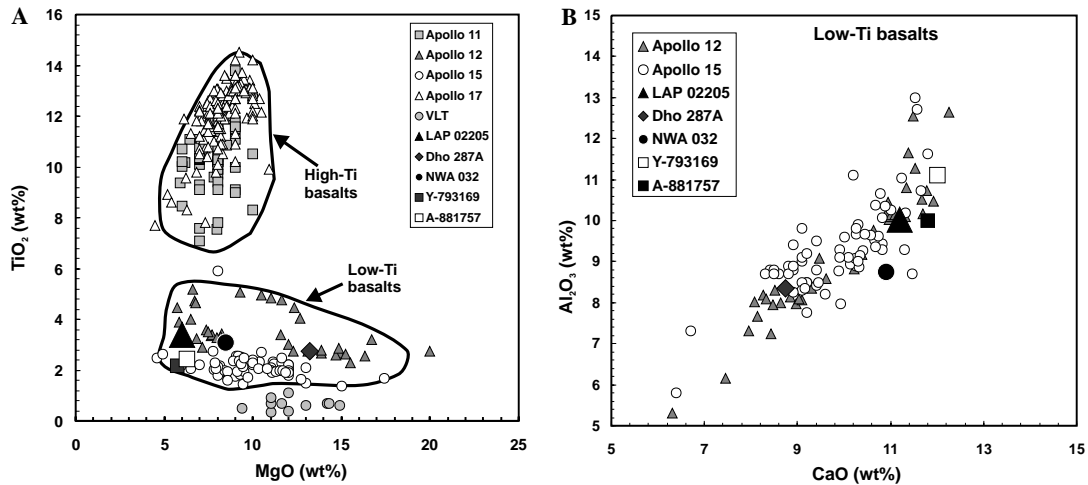
Fig. 7. Variation diagrams for selected whole rock major-element data for LAP 02205. Data for Apollo 11, 12, 15, and 17 mare basalts are also plotted for comparison. The inset in each figure shows the data set available for mare basalts from Apollo and Luna missions as compiled by Neal and Taylor (1992). (A) The MgO vs. TiO_2 plot confirms LAP as a low-Ti mare basalt, according to the classification of Neal and Taylor (1992). LAP is similar to the majority of Apollo 12 and 15 mare-basalt samples, but is relatively low in MgO. (B) the Al_2O_3 vs. CaO plot indicates that LAP is somewhat enriched in CaO and Al_2O_3 contents compared to most low-Ti mare basalts.
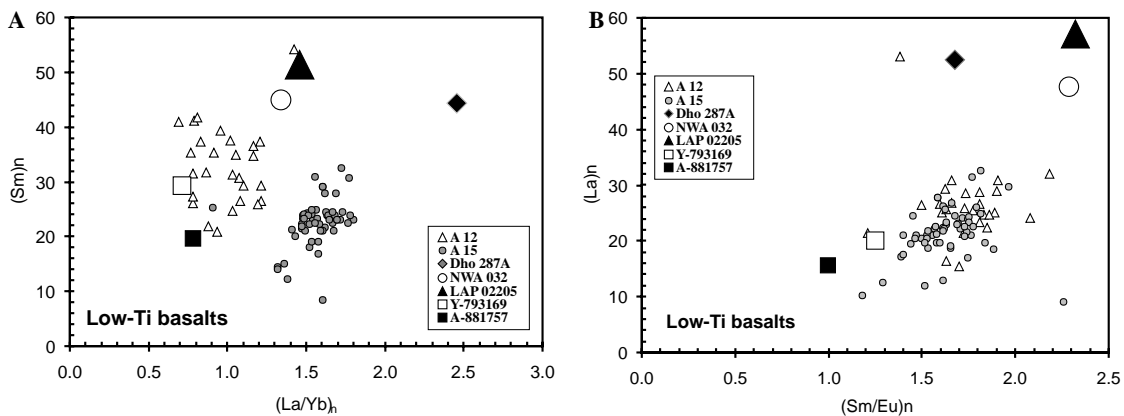

Fig. 8. Variation diagrams for selected whole-rock trace-element data for LAP 02205. Data for A 12 and A 15 mare basalts are also plotted for comparison. (A) The $(La/Yb)_n$ vs. $(Sm)_n$ plot highlights the REE-enriched nature of LAP. (B) The $(Sm/Eu)_n$ vs. $(La)_n$ plot highlights the negative Eu anomaly in LAP, typical of mare basalts. A close similarity between LAP and NWA 032 is apparent from both figures.
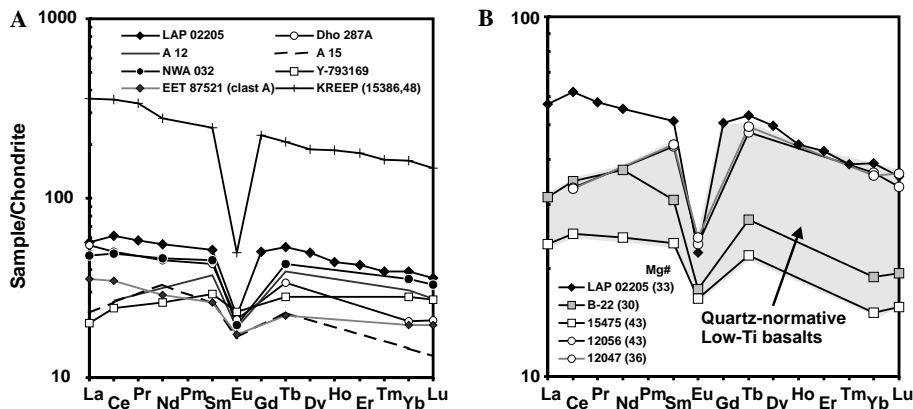

Fig. 9. (A) Chondrite-normalized plot of REEs in LAP 02205. Normalization values are from Anders and Grevesse (1989). Other mare-basalt meteorites, one representative analysis each of Apollo 12 and 15 mare basalts (12019, 15119; Table 3), and KREEP (15386; Neal and Kramer, 2003) are also plotted for comparison. (B) REE pattern of LAP 02205 compared with quartz-normative Apollo 12 basalts. The shaded region covers the range of REE contents shown by low-Ti quartz-normative basalts from the Apollo collection. Data for mare basalts plotted in this figure are given in Table 3.

Table 4
Platinum group element (PGE) abundances (in ppb) in LAP 02205

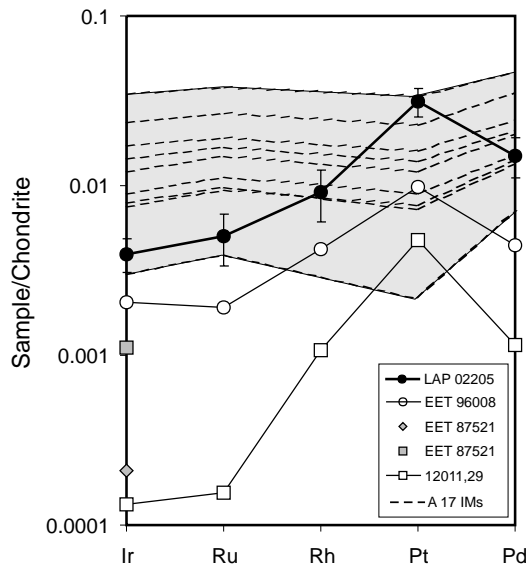|	LAP 02205	2σ	WITS-1 (analyzed)	2σ	WITS-1 (recommended)	2σ
Ir	1.8	0.4	2.1	0.6	1.6	0.2
Ru	3.6	1.2	4.5	3.9	5.1	1.2
Rh	1.2	0.4	3.1	2.1	1.3	0.2
Pt	31.5	6	8	1.2	11	2
Pd	8.3	2.2	8.9	3	7.9	0.9

Fig. 10. Chondrite-normalized PGE pattern for LAP 02205 compared with PGE patterns of Apollo 17 impact melt (IM) breccias studied by Norman et al. (2002) and other mare basaltic rocks. PGE data for A 12 basalt (12011,29) are our unpublished data (Ir = 0.06 ppb, Ru = 0.11 ppb, Rh = 0.14 ppb, Pt = 4.82 ppb, and Pd = 0.63 ppb), whereas data for mare basaltic meteorites EET 96008 and EET 87521 are from Anand et al. (2003c) and Warren and Kallemeyn (1991), respectively. LAP has a highly fractionated smooth chondrite-normalized pattern similar to those of EET 96008 and 12011,29. However, the platinum abundance in LAP basalt is comparable to some of the highest values seen in the impact melt breccias. The chondrite normalization values used here are from McDonough and Sun (1995).

pattern is approximately flat; consequently, these grains have some of the highest (La/Yb)$_n$ values. This is consistent with their highly evolved compositions. The lowest (La/Yb)$_n$ values are seen in high-Mg pigeonites (Fig. 11C), in agreement with petrographic observations and crystallization modeling that pigeonite was the earliest crystallizing phase in the LAP magma. The REE contents in plagioclase grains also show significant variation. All plagioclase grains have LREE-enriched patterns with large positive Eu anomalies (Fig. 11A). The overall REE abundance increases with decreasing plagioclase An content. Three olivine grains also show some variation in REE abundances; patterns are HREE-enriched with abundances of REE lighter than Gd below detection.

The REE data on apatite and whitlockite show smooth chondrite-normalized REE patterns between 10,000 and 20,000 times chondrite with strong negative Eu anomalies

(Fig. 11A). The REE concentrations are higher in whitlockite than in apatite, consistent with previous studies of lunar phosphates (e.g., Lindstrom et al., 1985; Neal and Taylor, 1991; Snyder and Taylor, 1992; Jolliff et al., 1993). However, the REE contents in LAP whitlockite and apatite are at the lower and higher ends, respectively, of known lunar compositions. This is due to a combination of small grain size (20–40 μm), especially for whitlockite (10–20 μm), and complex intergrowth of these two phases in LAP, making it difficult to avoid contamination by analyzing a mixture of the two phases during ion microprobe analysis.

If no equilibration of the REE has taken place, the REE compositions of individual minerals can be used to estimate the compositions of the liquid with which they were in equilibrium at the time of crystallization (e.g., McSween et al., 1996). Agreement between the bulk rock REE compositions and the estimated equilibrium melt composition for the earliest-formed minerals can indicate closed-system crystallization of the parental magma. We have calculated equilibrium melt compositions for the pigeonite, augite, and plagioclase from LAP 02205 with the lowest REE concentrations (i.e., those that formed earliest) and have compared them with the measured bulk-rock REE composition (Fig. 12). We used REE partition coefficients from McKay et al. (1986) for pigeonite and augite, and those from Phinney and Morrison (1990), for plagioclase (except for Eu, which is from Drake and Weill, 1975). The shaded area in Fig. 12 indicates the range of estimated equilibrium liquid compositions for the three minerals. The melts in equilibrium with early formed plagioclase and pyroxene are similar to each other, suggesting that the high-Mg pyroxenes and An-rich plagioclase co-crystallized from similar melts (Fig. 12). This is further supported by crystallization modeling (see next section) that predicts appearance of plagioclase on the liquidus almost immediately after pigeonite. The whole-rock REE pattern for LAP is also plotted in Fig. 12 and is similar to the calculated equilibrium melts. This observation supports the interpretation that the whole-rock composition of LAP 02205 reflects the original melt composition and that no cumulus phase is present in the rock sample.

4.3. Crystallization modeling

The modal mineralogy of LAP 02205 and its geochemical characteristics demonstrate the highly fractionated nature of the parental magma. The highest measured Fo content in LAP olivine cores (Fo 64) is a bit too high to be in equilibrium with our measured whole rock Mg# of 31.4. Using the TiO$_2$-calibrated K_d of 0.32 (Delano, 1980), the calculated Fo content of olivine that is in equilibrium with a whole rock Mg# 31.4 is approximately 60. Other investigators of LAP 02205 have reported Fo content in olivine cores as high as 67 (Chokai et al., 2004), which would suggest a xenocrystic origin for some of the high-Mg olivine cores. The skeletal nature of olivine grains

Table 5
REE abundances (in ppm) in silicate and phosphate minerals in LAP 02205 measured by SIMS

Pyroxene

	apx33	1σ	apx36	1σ	apx75	1σ	apx79	1σ	f2px34	1σ	f2px40	1σ	f2px49	1σ	f2px55	1σ	f2px57	1σ	f2px60	1σ	f2px66	1σ
La	1.39	0.08	0.31	0.03	0.06	0.01	0.13	0.01	0.42	0.05	7.43	0.30	0.14	0.02	0.29	0.04	0.07	0.01	0.39	0.05	0.82	0.05
Ce	5.77	0.27	1.16	0.08	0.26	0.02	0.64	0.05	1.87	0.18	24.93	0.78	0.67	0.06	1.44	0.12	0.35	0.02	2.28	0.18	3.64	0.20
Pr	1.27	0.07	0.31	0.02	0.06	0.01	0.15	0.02	0.42	0.05	4.73	0.23	0.15	0.02	0.36	0.03	0.10	0.01	0.50	0.05	0.71	0.05
Nd	7.68	0.26	1.97	0.09	0.39	0.02	0.98	0.05	2.62	0.17	20.90	0.60	1.04	0.05	2.16	0.12	0.66	0.03	2.89	0.16	4.99	0.17
Sm	3.58	0.23	0.99	0.09	0.28	0.03	0.53	0.05	1.64	0.16	7.91	0.49	0.65	0.06	1.14	0.12	0.39	0.04	1.54	0.13	2.77	0.13
Eu	0.17	0.02	0.05	0.01	0.01	0.00	0.03	0.01	0.09	0.02	0.54	0.08	0.04	0.01	0.06	0.01	0.03	0.01	0.06	0.02	0.17	0.02
Gd	5.47	0.46	2.09	0.19	0.46	0.04	1.07	0.09	2.27	0.30	10.30	0.84	0.98	0.10	2.28	0.22	0.70	0.07	2.30	0.24	3.48	0.29
Tb	1.47	0.10	0.35	0.04	0.11	0.01	0.20	0.02	0.61	0.08	2.50	0.21	0.25	0.02	0.57	0.06	0.16	0.02	0.63	0.06	0.78	0.06
Dy	10.71	0.39	3.46	0.14	1.12	0.04	2.07	0.09	4.04	0.21	16.59	0.59	2.05	0.10	3.74	0.19	1.41	0.06	3.99	0.22	5.73	0.23
Ho	2.24	0.16	0.75	0.06	0.29	0.03	0.44	0.04	0.90	0.09	3.30	0.19	0.46	0.04	0.76	0.07	0.31	0.02	0.71	0.07	1.19	0.08
Er	7.87	0.29	2.47	0.09	0.90	0.04	1.55	0.08	2.68	0.18	10.43	0.40	1.71	0.09	2.65	0.14	1.03	0.04	2.62	0.14	3.73	0.16
Tm	1.30	0.08	0.34	0.03	0.12	0.01	0.23	0.03	0.44	0.05	1.48	0.09	0.25	0.02	0.46	0.05	0.16	0.01	0.39	0.05	0.52	0.04
Yb	8.70	0.42	3.00	0.17	1.12	0.06	1.63	0.11	2.81	0.30	10.65	0.58	1.58	0.12	2.47	0.19	1.08	0.08	2.09	0.16	3.78	0.21
Lu	1.50	0.14	0.53	0.05	0.18	0.02	0.25	0.03	0.41	0.07	1.47	0.16	0.32	0.05	0.43	0.06	0.17	0.02	0.31	0.07	0.56	0.06
Wo	22.3		30.6		8.6		20.8		40.4		35.1		23.1		29.2		14.2		38.3		16.6	
En	4.4		22.1		57.9		36.6		5.9		8.5		39.8		43.7		54.9		40.0		34.1	

	f2px68	1σ	fpx123	1σ	fpx128	1σ	fpx130	1σ	fpx173	1σ	hpx40	1σ	hpx45	1σ	hpx64	1σ	hpx68	1σ	hpx94	1σ	jpx71	1σ
La	0.30	0.04	0.08	0.01	0.15	0.02	0.35	0.05	0.18	0.02	0.21	0.03	0.47	0.04	1.85	0.05	0.20	0.02	0.09	0.01	5.41	0.28
Ce	1.59	0.11	0.17	0.03	0.62	0.04	2.09	0.16	0.83	0.05	0.69	0.07	2.44	0.16	5.38	0.17	1.25	0.07	0.34	0.02	16.42	0.70
Pr	0.37	0.03	0.06	0.01	0.11	0.01	0.32	0.03	0.19	0.02	0.17	0.02	0.56	0.05	0.88	0.05	0.31	0.02	0.09	0.01	2.55	0.16
Nd	2.57	0.14	0.34	0.03	1.02	0.04	2.49	0.15	1.13	0.05	1.19	0.06	3.35	0.14	4.30	0.13	1.85	0.08	0.58	0.03	13.41	0.47
Sm	1.23	0.13	0.24	0.04	0.53	0.04	1.31	0.12	0.61	0.04	0.51	0.07	1.72	0.12	1.68	0.08	1.17	0.07	0.38	0.03	4.79	0.30
Eu	0.08	0.01	0.01	0.00	0.03	0.01	0.11	0.02	0.05	0.01	0.03	0.01	0.12	0.01	0.08	0.01	0.04	0.01	0.03	0.01	0.38	0.06
Gd	2.91	0.24	0.32	0.10	1.01	0.09	2.41	0.23	1.25	0.10	1.32	0.17	2.30	0.24	2.30	0.20	2.15	0.17	0.53	0.07	6.86	0.60
Tb	0.56	0.06	0.09	0.02	0.27	0.02	0.54	0.05	0.29	0.02	0.19	0.04	0.59	0.05	0.59	0.04	0.46	0.04	0.17	0.01	1.62	0.12
Dy	4.02	0.20	0.95	0.06	2.36	0.08	3.88	0.22	2.03	0.09	1.90	0.10	4.49	0.20	4.42	0.18	4.17	0.17	1.36	0.06	9.60	0.39
Ho	0.90	0.08	0.24	0.02	0.63	0.04	0.72	0.10	0.47	0.03	0.45	0.04	0.90	0.07	1.01	0.07	0.95	0.07	0.30	0.02	2.18	0.14
Er	3.08	0.16	0.70	0.05	1.91	0.06	3.08	0.18	1.62	0.06	1.46	0.08	2.84	0.15	3.03	0.13	3.32	0.15	0.89	0.05	6.09	0.29
Tm	0.50	0.05	0.13	0.01	0.29	0.02	0.34	0.04	0.25	0.01	0.19	0.02	0.40	0.03	0.55	0.04	0.44	0.03	0.17	0.01	0.84	0.07
Yb	3.42	0.21	0.79	0.08	2.30	0.11	2.52	0.27	1.65	0.09	1.65	0.13	2.75	0.19	3.30	0.17	3.63	0.27	1.11	0.07	6.82	0.36
Lu	0.53	0.07	0.15	0.03	0.42	0.04	0.34	0.07	0.32	0.04	0.32	0.05	0.40	0.06	0.57	0.04			0.19	0.02	1.13	0.10
Wo	24.2		0.9		9.9		35.4		18.7		33.2		36.9		20.9		16.4		21.1		17.9	
En	29.0		46.0		40.5		41.0		41.8		44.4		36.2		21.3		3.7		47.8		14.4	

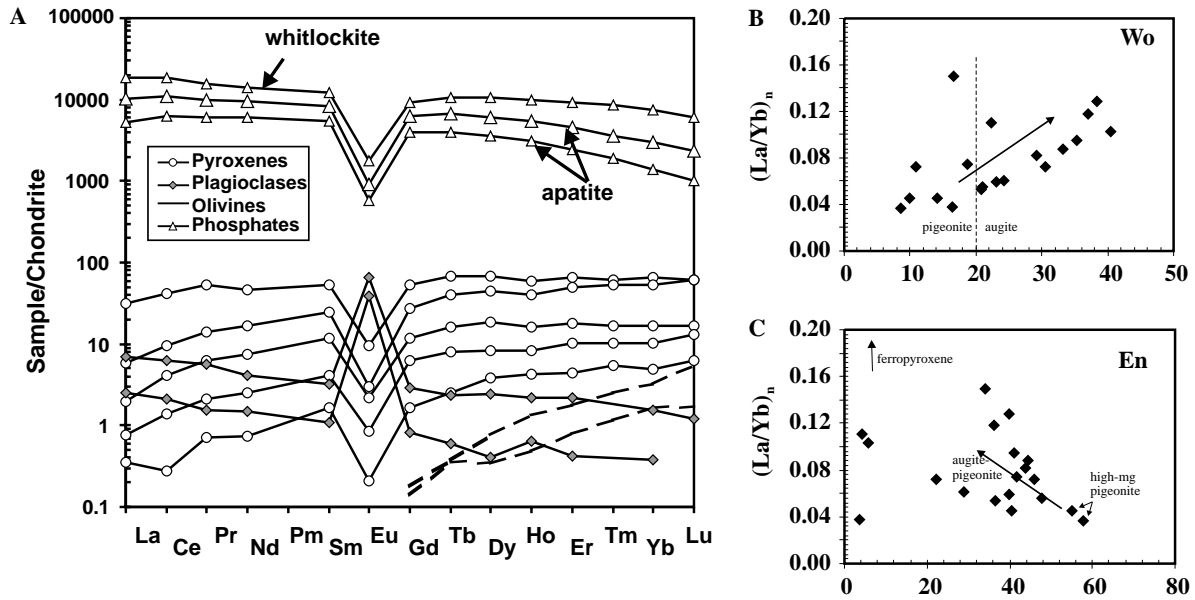|	Olivine						Plagioclase												Phosphates					
	a2ol16	1σ	a2ol23	1σ	hol13	1σ	f2pl82	1σ	f2pl88	1σ	f2pl95	1σ	jpl49	1σ	gpl8	1σ	gpl9	1σ	p2Ap1	1σ	p2Wh2	1σ	p7Ap10	1σ
La							0.62	0.05	0.83	0.05	0.52	0.03	1.66	0.08	0.68	0.06	0.59	0.03	1225	14	4400	27	2408	15
Ce							1.49	0.10	2.16	0.12	1.28	0.08	3.85	0.16	1.64	0.09	1.25	0.06	3723	28	11264	48	6614	28
Pr							0.19	0.02	0.27	0.02	0.14	0.01	0.50	0.04	0.20	0.02	0.14	0.01	543	9	1396	14	888	9
Nd							0.67	0.04	1.20	0.05	0.50	0.04	1.87	0.07	0.82	0.04	0.67	0.03	2695	27	6376	41	4355	26
Sm							0.20	0.03	0.28	0.04	0.13	0.03	0.47	0.04	0.15	0.03	0.16	0.02	793	22	1782	33	1217	21
Eu							1.36	0.08	1.80	0.09	1.54	0.06	3.64	0.14	1.99	0.09	2.17	0.08	32	2	100	4	51	2
Gd	0.04	0.01	0.03	0.01			0.26	0.04	0.42	0.05	0.16	0.03	0.56	0.05	0.18	0.03	0.16	0.02	789	25	1836	37	1247	23
Tb	0.01	0.00	0.01	0.00	0.02	0.00	0.04	0.01	0.06	0.01	0.03	0.01	0.09	0.01	0.03	0.01	0.02	0.01	145	6	378	10	246	6
Dy	0.18	0.01	0.08	0.01	0.11	0.01	0.16	0.02	0.43	0.03	0.09	0.02	0.59	0.03	0.18	0.02	0.10	0.01	856	16	2539	27	1476	16
Ho	0.07	0.01	0.03	0.01	0.03	0.00	0.04	0.01	0.12	0.01	0.02	0.01	0.12	0.01	0.05	0.01	0.04	0.01	173	6	547	11	302	6
Er	0.28	0.02	0.13	0.01	0.10	0.01	0.08	0.02	0.30	0.03	0.06	0.02	0.34	0.02	0.10	0.02	0.07	0.01	383	11	1463	21	715	11
Tm	0.06	0.01	0.03	0.01															45	3	208	7	87	3
Yb	0.53	0.03	0.27	0.03	0.20	0.02	0.05	0.02	0.31	0.04	0.07	0.02	0.25	0.03	0.07	0.02	0.06	0.01	223	11	1208	23	491	12
Lu	0.13	0.01	0.04	0.01	0.04	0.01			0.05	0.01					0.03	0.01	0.01	0.01	25	4	147	8	57	4
Fo	42.4		58.3		62.4																			
An							89.2		88.6		86.9		84.6		87.4		88.2							

Errors are 1σ.

Fig. 11. (A) Chondrite-normalized plot of REE abundances in silicate and phosphate grains from LAP. The REEs in pyroxene grains display a large variation with deep negative Eu anomalies. The REEs in plagioclase and olivine also vary significantly. For clarity, only the most representative REE patterns are shown that cover the measured range for each mineral type. (B and C) $(La/Yb)_n$ vs. Wo and En, respectively, for LAP pyroxenes, illustrating the control of pigeonite and augite crystallization on $(La/Yb)_n$ values at a given Wo and En content.
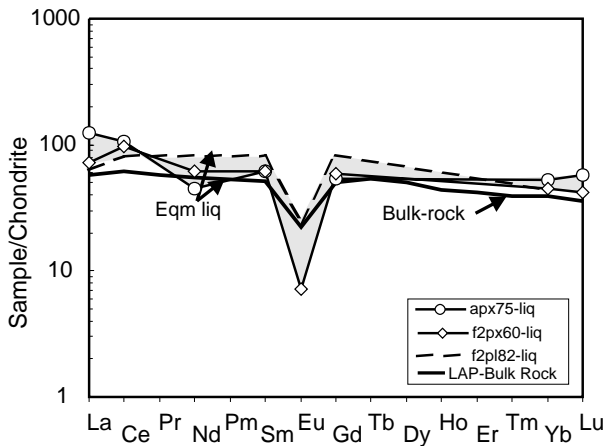
Fig. 12. Chondrite-normalized REE patterns of the calculated e parental melts in equilibrium with the earliest formed pyroxenes and plagioclase in LAP. The early formed pyroxenes and plagioclase are in equilibrium with similar parental melts, which are also similar to the measured bulk-rock REE patterns.

Fig. 13. Results of equilibrium crystallization modeling of the bulk rock composition of LAP 02205, using the MELTS software of Ghiorso and Sack (1995). The measured compositional ranges of LAP silicates are shown in the small inset at the top right. Bars depict relative timing between the appearances of observed mineral phases in LAP onto the liquidus.

and the reaction relationship with pigeonite are in agreement with this possibility. Nevertheless, as discussed earlier, preservation of Fe–Mg zoning in LAP olivines could only have occurred if they were derived from a slightly more magnesian magma not long before the onset of LAP magma crystallization. Thus, there might be a genetic link between the cores of such olivine grains and the LAP basalt through fractional crystallization of a primitive magma.

The bulk-rock composition of LAP 02205 (Table 3) has been modeled using the MELTS software of Ghiorso and Sack (1995). Results of equilibrium crystallization modeling

are presented in the form of bar diagrams in Fig. 13. Modeling was performed starting with a liquidus temperature of 1200 °C and oxygen fugacity equivalent to a log unit below the Iron–Wustite buffer (i.e., IW-1). The equilibrium crystallization modeling provides a good match between the predicted and observed compositional ranges for the majority of mineral phases, but fails to predict the observed Fo contents of the olivine cores, supporting our interpretation that these high-Mg cores may be xenocrysts. We also modeled the bulk composition of LAP reported by Jolliff et al.

Table 6
U and Pb isotopic values in LAP 02205 phosphates as measured by SHRIMP

	$^{238}U/^{206}Pb$	1σ	$^{207}Pb/^{206}Pb$	1σ	$^{204}Pb/^{206}Pb$	1σ	$^{204}Pb/^{208}Pb$	1σ	U (ppm)	Th (ppm)
LAP-K	1.280	0.143	0.2510	0.0068	0.000308	0.000099	0.000535	0.000171	75	188
LAP-P	1.543	0.027	0.2308	0.0021	0.000180	0.000039	0.000298	0.000064	96	359
LAP-ap3.1	1.208	0.278	0.2596	0.0131	0.000439	0.000150	0.000926	0.000324	73	207
LAP-ap3.2	1.191	0.452	0.2843	0.0304	0.000205	0.000094	0.000324	0.000152	70	330
LAP-ap4.1	1.326	0.100	0.2282	0.0065	0.000075	0.000084	0.000106	0.000120	72	285
LAP-ap4.2	1.183	0.109	0.2423	0.0041	0.000232	0.000070	0.000275	0.000083	65	347
LAP-ap5	1.143	0.291	0.2463	0.0045	0.000225	0.000049	0.000336	0.000075	60	303

Errors are 1σ.

(2004), which confirms our results and excludes the possibility of heterogeneous sampling of the LAP 02205.

4.4. U–Pb age dating of phosphates

The age of a lunar basalt can potentially yield important clues about its source location. It can also help in the pairing of meteorites. We previously published the first U–Th–Pb dates derived from phosphates from a lunar meteorite (Anand et al., 2003c). We have followed up on this unique technique to determine the U–Pb ages of phosphate grains in LAP as a first approximation of its crystallization age. The main advantage of our "total U–Pb isochron method" lies in the fact that this does not require any assumption of initial lead composition, which is model dependent (Terada et al., 2003; Terada and Sano, 2004). In addition, this is a relatively rapid method of dating phosphate grains, 'in-situ,' in basaltic samples without destroying much material and preserving the spatial context among various analyzed spots in a polished section. Thus, one of the aims of the present study was to use SHRIMP-derived data from phosphate mineral grains in LAP 02205 to place this sample within the chronologic context of its lunar origin. Due to the very small size of whitlockite crystals, it was only possible to determine U–Pb ages for apatite grains using this method.

U and Th concentrations, $^{238}U/^{206}Pb$, $^{207}Pb/^{206}Pb$, $^{204}Pb/^{206}Pb$, and $^{204}Pb/^{208}Pb$ ratios of apatites in LAP are listed in Table 6. Average Th and U concentrations in these phosphates vary from ∼200 to 350 ppm and are significantly higher than those in ordinary chondrites (Crozaz et al., 1987). This could simply be due to the fact that LAP phosphates were derived from a fractionated magma, containing higher concentrations of incompatible trace elements such as U and Th compared to chondrites. Both U and Th are highly enriched in LAP phosphates (Table 6) when compared with their concentration in the whole rock (Th = 2.33 ppm and U = 0.55 ppm; Th/U = 4.2). The Th/U ratios in apatites vary from 2.5 to 5 with an average value of ∼4, similar to those seen in other lunar basaltic meteorites (e.g., EET 96008; Anand et al., 2003c).

We have calculated a "total Pb/U isochron age" from the apatite data in $^{238}U/^{206}Pb$–$^{207}Pb/^{206}Pb$–$^{204}Pb/^{206}Pb$ space, using Isoplot/Ex v. 3.0 program (Ludwig, 2001). The linear regression in the 3D diagram intercepts with the U–Pb Concordia line at 2929 ± 150 Ma (2σ), taken as the minimum crystallization age of the lunar basalt LAP 02205 (Fig. 14). Although shock effects are present in LAP, they are less intense (e.g., lack of large-scale mask-elynitization of plagioclase) than those seen in other mare basalt meteorites, such that the U–Pb systematics in phosphates were possibly not disturbed. Thus, the U–Pb radiometric age may be close to a true crystallization age. In a pioneering study using SHRIMP, Sano et al. (2000) performed U–Th–Pb dating of phosphates in Shergotty, a strongly shocked (e.g., total maskelynitization of plagioclase) martian meteorite and obtained crystallization ages similar to those derived from other isotopic systems. However, because of the controversy surrounding the formation age of Shergotty, they were cautious in interpreting their results and suggested that this age could be either the age of the primary crystallization of the apatites or the age of the shock metamorphic event, which was associated with a temperature of ∼900 °C, interpreted to be the closure temperature of U–Pb system in shergotty apatites (Sano et al., 2000). In the present case, however, we believe that the U–Pb age of apatites is most likely to be the original crystallization age from the LAP magma. This is supported by its close similarity to another lunar meteorite, NWA 032, which has a similar Ar–Ar age (2.8 Ga) (Fernandes et al., 2003). Recently, Nyquist et al. (2005) also presented Sm–Nd, Rb–Sr, and Ar–Ar ages for the LAP basalt, with a maximum crystallization age of 3.1 Ga, based on Sm–Nd isotopic systematics and slightly younger ages of around 2.9 Ga based upon Rb–Sr and Ar–Ar isotopic dating techniques. The younger ages have been interpreted as being due to secondary events soon after the formation of the rock. These ages are similar to our U–Pb data and, when the errors are taken into account, the U–Pb ages are comparable to the Sm–Nd crystallization age of Nyquist et al. (2005), providing confidence in the use of U–Pb dating technique that we have pioneered.

5. Pairing with other mare basalts and lunar source region

One of the aims in lunar-meteorite research is to compare and contrast the mineralogy and petrology of a new mare basalt with those of existing mare basalts, from Apollo and Luna missions, as well as with those of other lunar-basalt samples to infer possible source regions for the new
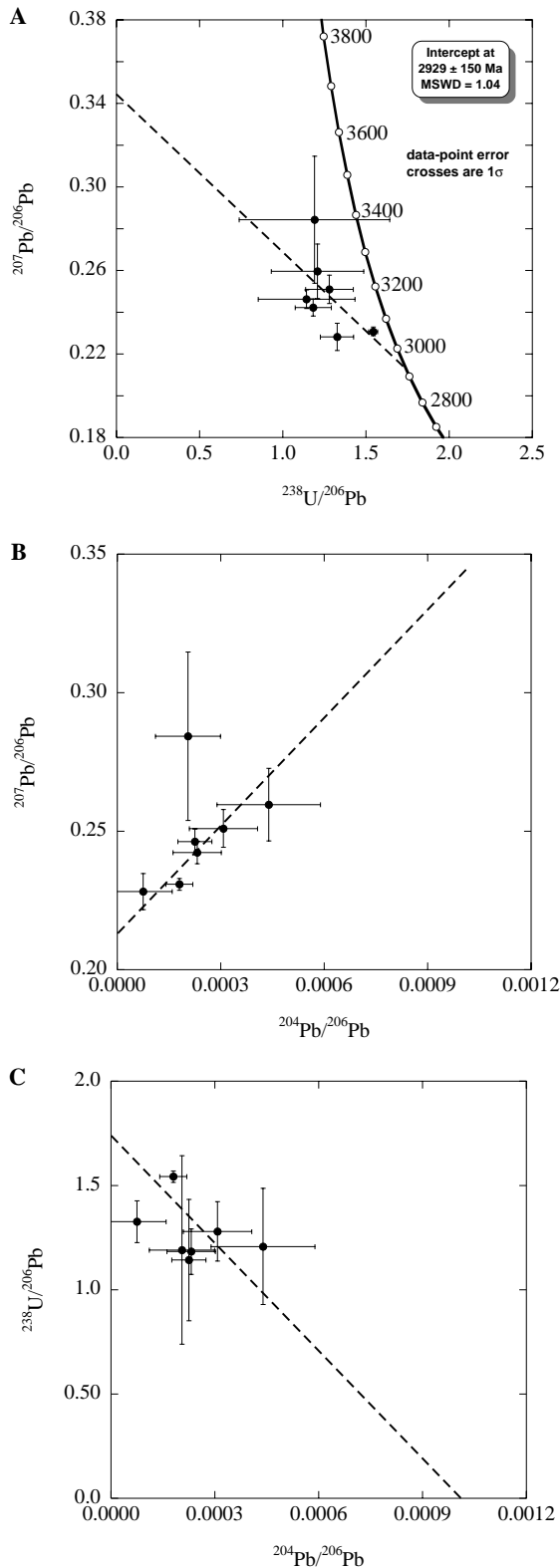
Fig. 14. A three-dimensional linear regression of apatite in the lunar meteorite LAP 02205 for the total Pb/U isochron. (A) All data are projected onto the $^{238}U/^{206}Pb$–$^{207}Pb/^{206}Pb$ plane. (B and C) are the other two planes of the cube. Errors are portrayed at the 1σ level. The dotted line shows the best fit by the Isoplot/Ex v. 3.0 (Ludwig, 2001). In (A), the intersection between the dashed isochron line and concordia curve (at 2929 Ma) is the corrected data ($^{207}Pb^*/^{206}Pb^*$) along the isochron line, taken as the crystallization age of the meteorite.

meteorite. This exercise helps not only to understand the pairing and source area location of a particular meteorite, but also helps to place the petrogenetic history of a sample in a wider geological context of lunar magma genesis.

LAP 02205 has unique mineralogical and geochemical characteristics, which have not been previously documented in any single known mare basalt. In our preliminary investigation of LAP 02205 (Anand et al., 2004), we suggested that this rock has some similarity with Apollo 12 and 15 low-Ti mare basalts from Apollo collections, especially the quartz-normative, pyroxene-phyric, A 15 basalts (e.g., 15075; Taylor and Misra, 1975). Mikouchi et al. (2004) and Chokai et al. (2004) have suggested that texturally LAP is most similar to Dho 287A. In terms of mineral chemistry, they considered LAP to be most similar to A 12 ilmenite basalt, 12056. Similarly, Righter et al. (2004) found some mineralogic similarity between LAP and the A 12 ilmenite basalts, particularly 12051. Joy et al. (2004) compared LAP to some low-Ti feldspathic basalts retrieved from the Luna 16 mission. They also considered A 12 pigeonite basalts as another possibility. Based on Nd and Sr isotopic composition, Nyquist et al. (2005) suggested a resemblance of LAP 02205 with Apollo 12 olivine basalts. Among mare basalt meteorites, based on major- and trace-element chemistry (e.g., similar Sc, Co contents, and Th/Sm ratio), Korotev et al. (2004) and Jolliff et al. (2004) argued for a possible launch pairing of LAP and mare-basalt meteorite NWA 032. The whole rock major- and trace-element compositions, as well as the U–Pb age, indeed, suggest a close similarity to NWA 032 (Fagan et al., 2002; Fernandes et al., 2003; Korotev et al., 2004). However, when looked in greater detail (e.g., level of incompatible trace element enrichment), LAP and NWA 032 cannot simply be related by fractional crystallization of a primitive melt. Nevertheless, these two meteorites share most geochemical signatures and it is entirely possible that both rocks were derived from similar source regions, if not from the same lava flow.

Despite differing opinions about the similarity of LAP to different types of mare basalts, most authors do agree that the western mare region on the Moon is a possible source region for this meteorite (Hiesinger and Head, 1999). This conclusion is bolstered by radiogenic age data on LAP 02205, which requires a source Maria with a relatively young age (<3.1 Ga). The high REE contents, the young age of ~3.0 Ga, and close similarity to NWA 032 are indicative of a source terrain close to the Apollo 12 site, possibly in Mare Insularum, Cognitum, Nubium or from the vicinity of Oceanus Procellarum and Mare Imbrium (Nyquist et al., 2005).

6. Summary

LAP 02205 is a new low-Ti mare basalt, which is unique in several respects compared to other lunar basalts. In terms of texture and mineralogy LAP is similar to Apollo 12 and Apollo 15 low-Ti mare basalts, albeit highly frac-

tionated. Pyroxene compositions are typical for low-Ti mare basalts, with progressive Fe-enrichment towards pyroxferroite. The high degree of fractionation is also evident in the unusually high abundance of mesostasis. Shock features are present in the meteorite in the form of mosaic fractures and twinning in pyroxenes, local melt pockets, and step fractures in ilmenites. However, plagioclase has retained its primary twinningm suggesting the rock was mildly shocked compared to most lunar mare basaltic meteorites.

At the individual mineral scale, pyroxene grains are LREE enriched and display a large range of REE abundances with deep negative Eu anomalies. Plagioclase grains also have variable REE abundances, with pronounced positive Eu anomalies. The calculated REE contents of the melts in equilibrium with the earliest formed pyroxenes and plagioclase are similar to the measured bulk-rock REE contents, thereby providing evidence for a closed system magmatic evolution of this rock.

In terms of bulk-rock major element contents, LAP 02205 has lower MgO contents than most other mare basalts with abundant free silica, making it a highly evolved basalt. It also has the highest REE abundances among all low-Ti mare basalts. LAP and NWA 032 have similar REE contents and Th/Sm ratio, and share many geochemical features. However, the LAP basalt cannot be derived from a simple fractionation of an NWA 032 type melt. The bulk-rock PGE contents in LAP basalt are highly enriched and form a smooth pattern on a chondrite-normalized plot, similar to other pristine low-Ti mare basalts from Apollo collections. This argues against any 'extraneous' meteoritic contamination and suggests a PGE-enriched source region for this mare basalt.

The U–Pb age of 2.9 Ga of LAP phosphates, if taken as crystallization age of the basalt, provides further evidence for extended magmatic activity on the Moon. This age makes LAP the 3rd youngest mare basalt known to date; the other two being NWA 032 (2.8 Ga) and NWA 773 (2.91 Ga) (Fernandes et al., 2003).

The western hemisphere on the nearside of the Moon is a possible source region for the LAP basalt, as suggested by the high abundances of REEs and young magmatic age (Hiesinger and Head, 1999). The overall mineralogical and geochemical characteristics of LAP 02205 are indicative of a new variant of low-Ti mare basalts, similar in some aspects to those from the Apollo 12 and 15 collections, and closest to lunar meteorite NWA 032, albeit LAP is more fractionated.

Acknowledgments

Associate editor: David W. Mittlefehldt

References

Alexander, C.M.O.D., 1994. Trace element distributions within ordinary chondrite chondrules: implications for chondrule formation conditions and precursors. *Geochim. Cosmochim. Acta* **58**, 3451–3467.

Amossé, J., Allibert, M., 1993. Partitioning of iridium and platinum between metals and silicate melts: evidence for passivation of the metals depending on fO_2. *Geochim. Cosmochim. Acta* **57**, 2395–2398.

Anand, M., Taylor, L.A., Misra, K.C., Demidova, S.I., Nazarov, M.A., 2003a. KREEPy lunar meteorite Dhofar 287A: a new lunar basalt. *Meteorit. Planet. Sci.* **38**, 485–499.

Anand, M., Taylor, L.A., Nazarov, M.A., Patchen, A., 2003b. Petrologic comparisons of lunar mare basalt meteorites Dh-287A and NWA 032. In: *Lunar Planet. Sci. Conf. XXXIV, Abstract No. 1787.* Lunar Planetary Institute, Houston (CD-ROM).

Anand, M., Taylor, L.A., Neal, C.R., Snyder, G.A., Patchen, A., Sano, Y., Terada, K., 2003c. Unraveling the complex origin of lunar meteorite EET 96008. *Geochim. Cosmochim. Acta* **67**, 3499–3518.

Anand, M., Taylor, L.A., Neal, C., Patchen, A., Kramer, G., 2004. Petrology and geochemistry of LAP 02205; a new low-Ti mare-basalt meteorite. In: *Lunar Planet. Sci. Conf. XXXV, Abstract No. 1626.* Lunar Planetary Institute, Houston (CD-ROM).

Anders, E., Grevesse, N., 1989. Abundances of the elements: meteoritic and solar. *Geochim. Cosmochim. Acta* **53**, 197–214.

Anders, E., Ganapathy, R., Keays, R.R., Laul, J.C., Morgan, J.W., 1971. Volatile and siderophile elements in lunar rocks: comparison with terrestrial and meteoritic basalts. *Proc. Lunar Sci. Conf. 2nd*, 1021–1036.

Baedecker, P.A., Schaudy, R.S., Elzie, J.L., Kimberlin, J., Wasson, J.T., 1971. Trace element studies of rocks and soils from Oceanus Procellarum and Mare Tranquilitatis. *Proc. Lunar Sci. Conf. 2nd*, 1037–1061.

Borisov, A., Nachtwweyth, K. 1998. Ru solubility in silicate melts: experimental results in oxidizing region (abstract). *Lunar Planet. Sci. XXIX* #1320.

Borisov, A., Palme, H., 1995. The solubility of iridium in silicate melts: new data from experiments with $Ir_{10}Pt_{90}$ alloys. *Geochim. Cosmochim. Acta* **59**, 481–485.

Borisov, A., Palme, H., 1997. Experimental determination of the solubility of platinum in silicate melts. *Geochim. Cosmochim. Acta* **61**, 4349–4357.

Borisov, A., Palme, H., 1998. Experimental determination of the solubility of Os metal/silicate partitioning. *Neues Jar. Min. Abstract* **172**, 347–356.

Borisov, A., Walker, R.J., 2000. Os solubility in silicate melts: new efforts and results. *Am. Miner.* **85**, 912–917.

Borisov, A., Palme, H., Spettel, B., 1994. Solubility of palladium in silicate melts: implications for core formation in the earth. *Geochim. Cosmochim. Acta* **58**, 705–716.

Chokai, J., Mikouchi, T., Arai, T., Monkawa, A., Koizumi, E., Miyamoto, M. 2004. Mineralogical comparison between LAP 02205 and lunar mare basalts (abstract). Ant. Met. XXVIII, pp. 4–5, National Institute of Polar Research, Tokyo.

Collins, S.J., Righter, K., Brandon, A. 2005. Mineralogy, petrology and oxygen fugacity of the LaPaz Ice Field lunar basaltic meteorites and the origin and evolution of evolved lunar basalts. In Lunar Planet. Sci. Conf. XXXVI, Abstract No. 1141. Lunar Planetary Institute, Houston (CD-ROM).

Crozaz, G., de Chazal, S., Lundberg, L.L., Zinner, E., Pellas, P., Bourt-Denise, M., 1987. Actinides and rare earth elements in chondrites. *Meteoritics* **22**, 362–363.

Crozaz, G., Floss, C., Wadhwa, M., 2003. Chemical alteration and REE mobilization in meteorites from hot and cold deserts. *Geochim. Cosmochim. Acta* **67**, 4727–4741.

Day, J.M.D., Pearson, D.G., Taylor, L.A., 2005. ^{187}Re–^{187}Os isotope disturbance in LaPaz Mare basalt meteorites. In: *Lunar Planet. Sci. Conf. XXXVI, Abstract No. 1424.* Lunar Planetary Institute, Houston (CD-ROM).

Delano, J.W., 1980. Chemistry and liquidus phase relations of Apollo 15 red glass: implications for the deep lunar interior. *Proc. Lunar Planet. Sci. Conf. 11th*, 251–288.

Delano, J.W., Ringwood, A.E., 1978. Siderophile elements in the lunar highlands: nature of the indigenous component and implications for the origin of the Moon. *Proc. Lunar Planet. Sci. Conf. 9th*, 111–119.

Drake, M.J., Weill, D.F., 1975. The partition of Sr, Ba, Ca, Y, Eu^{2+}, Eu^{3+}, and other REE between plagioclase feldspar and magmatic silicate liquid: an experimental study. *Geochim. Cosmochim. Acta* **39**, 689–712.

El Goresy, A., 1976. Oxide minerals in lunar rocks. In: Rumble, D. (Ed.), *Oxide minerals*, Mineralogical Society of America. pp. EG1–43.

Ely, J.C., Neal, C.R., O'Neill Jr., J.A., Jain, J.C., 1999. Quantifying the platinum group elements (PGEs) and gold in geological samples using cation exchange pretreatment and ultrasonic nebulization inductively coupled plasma-mass spectrometry (USN-ICP-MS), *Chem. Geol.* (**157**), 219–234.

Ertel, W., O'Neill, H.St.C., Sylvester, P.J., Dingwell, D.B., 1999. Solubilities of Pt and Rh in a haplobasaltic silicate melt at 1300ûC. *Geochim. Cosmochim. Acta* **63**, 2439–2449.

Fagan, T.J., Taylor, G.J., Keil, K., Bunch, T.E., Wittke, J.H., Korotev, R.L., Jolliff, B.L., Gillis, J.J., Haskin, L.A., Jarosewich, E., Clayton, R.N., Mayeda, T., Fernandes, V.A., Burgess, R., Turner, G., Eugster, O., Lorenzetti, S., 2002. Northwest Africa 032: product of lunar volcanism. *Meteorit. Planet. Sci.* **37**, 371–394.

Fernandes, V.A., Burgess, R., Turner, G., 2003. ^{40}Ar–^{39}Ar chronology of lunar meteorites Northwest Africa 032 and 773. *Meteorit. Planet. Sci.* **38**, 555–564.

Floss, C., Crozaz, G., 1991. Ce anomalies in the LEW 85300 eucrite: evidence for REE mobilization during Antarctic weathering. *Earth Planet. Sci. Lett.* **107**, 13–24.

Floss, C., Jolliff, B., 1998. Rare Earth Element Sensitivity Factors in Calcic Plagioclase (Anorthite). Secondary Ion Mass Spectrometry, SIMS XI, 785–788.

Ghiorso, M.S., Sack, R.O., 1995. Chemical mass transfer in magmatic processes. IV.A Revised and internally consistent thermodynamic model for the interpolation and extrapolation of liquid–solid equilibria in magmatic systems at elevated temperatures and pressures. *Contrib. Miner. Petrol.* **119**, 197–212.

Giguere, T., Taylor, G.J., Hawke, B.R., Lucey, P.G., 2000. The titanium contents of lunar mare basalts. *Meteorit. Planet. Sci.* **35**, 193–200.

Grove, T., Walker, D., 1977. Cooling histories of Apollo 15 quartz-normative basalts. *Proc. Lunar Sci. Conf. 8th*, 1501–1520.

Hiesinger, H., Head, J.W., III 1999. Ages of Oceanus Procellarum basalts and other nearside mare basalts. Workshop on the New Views of the Moon II: Understanding the Moon Through the Integration of Diverse Datasets. *Abstract No. 8030.* Lunar Planetary Institute, Houston (CD-ROM).

Hess, P.C., Rutherford, M.J., Campbell, H.W., 1978. Ilmenite crystallization in non-mare basalt: genesis of KREEP and high-Ti mare basalt. *Proc. Lunar Sci. Conf. 9th*, 705–724.

Hsu, W. 1995. Ion Microprobe Studies of the Petrogenesis of Enstatite Chondrites and Eucrites. Ph.D. thesis. Washington University, St. Louis.

Jolliff, B.L., Haskin, L.A., Colson, R.O., Wadhwa, M., 1993. Partitioning in REE-saturating minerals: Theory, experiment, and modeling of whitlockite, apatite, and evolution of lunar residual magmas. *Geochim. Cosmochim. Acta* **57**, 4069–4094.

Jolliff, B.L., Zeigler, R.A., Korotev, R.L., 2004. Petrography of lunar meteorite LAP 02205, a new low-Ti basalt possibly launch paired with NWA 032. In: *Lunar Planet. Sci. Conf. XXXV, Abstract No. 1438.* Lunar Planetary Institute, Houston (CD-ROM).

Joy, K.H., Crawford, I.A., Russell, S.S., Kearsley, A. 2004. Mineral chemistry of LaPaz Ice Field 02205—A new lunar basalt. In *Lunar Planet. Sci. Conf. XXXV, Abstract No. 1545.* Lunar Planetary Institute, Houston (CD-ROM).

Koeberl, C., Kurat, G., Brandstatter, F., 1993. Gabbroic lunar meteorites Asuka-881757 (Asuka-31) and Yamato-793169: Geochemical and mineralogical study. In: *NIPR Symp. Antarct. Meteorites,* VI, pp. 14–34.

Korotev, R.L., Zeigler, R.A., Jolliff, B.L., 2004. Compositional constraints on the launch pairing of LAP 02205 and PCA 02007 with other lunar meteorites. In: *Lunar Planet. Sci. Conf. XXXV, Abstract No. 1416.* Lunar Planetary Institute, Houston (CD-ROM).

Lindstrom, M.M., Crozaz, G., Zinner, E., 1985. REE in phosphates from lunar highland cumulates: an ion microprobe study (abstract). *Lunar Planet Sci. XVI*, 493–494.

Ludwig, K.R., 2001. *Users Manual for Isoplot/Ex v. 2.49: A Geochronological Toolkit for Microsoft Excel.* Berkeley Geochronology Center Special Publication No. 1a.

McDonough, W.F., Sun, S.-S., 1995. The composition of the Earth. *Chem. Geol.* **120**, 223–254.

McKay, G., Wagstaff, J., Yang, S.-R., 1986. Clinopyroxene REE distribution coefficients for shergottites: the REE content of the Shergotty melt. *Geochim. Cosmochim. Acta* **50**, 927–937.

McSween, H.Y., Eisenhour, D.D., Taylor, L.A., Wadhwa, M., Crozaz, G., 1996. QUE94201 shergottite: crystallization of a Martian basaltic magma. *Geochim. Cosmochim. Acta* **60**, 4563–4569.

Mikouchi, T., Chokai, J., Arai, T., Koizumi, E., Monkawa, A., Miyamoto, M., 2004. LAP 02205 lunar meteorite: lunar mare basalt with similarities to the Apollo 12 ilmenite basalt. In: *Lunar Planet. Sci. Conf. XXXV, Abstract No. 1548.* Lunar Planetary Institute, Houston (CD-ROM).

Neal, C.R., 2001. Interior of the Moon: the presence of garnet in the primitive deep lunar mantle. *J. Geophys. Res. Planet* **106**, 27865–27885.

Neal, C.R., Kramer, G. 2003. The composition of KREEP: A detailed study of KREEP basalt 15386. *In Lunar Planet. Sci. Conf. XXXIV, Abstract No. 2023.* Lunar Planetary Institute, Houston (CD-ROM).

Neal, C.R., Taylor, L.A., 1989. Metasomatic products of the lunar magma ocean: The role of KREEP dissemination. *Geochim. Cosmochim. Acta* **53**, 529–541.

Neal, C.R., Taylor, L.A., 1991. Evidence for metasomatism of the lunar highlands and the origin of whitlockite. *Geochim. Cosmochim. Acta* **55**, 2965–2980.

Neal, C.R., Taylor, L.A., 1992. Petrogenesis of mare-basalts: a record of lunar volcanism. *Geochim. Cosmochim. Acta* **56**, 2177–2211.

Neal, C.R., Hacker, M.D., Snyder, G.A., Taylor, L.A., Liu, Y.-G., Schmitt, R.A., 1994. Basalt generation at the Apollo 12 site, Part 1: new data, classification, and re-evaluation. *Meteoritics* **29**, 334–348.

Neal, C.R., Ely, J.C., Jain, J.C., 2001. The siderophile element budget of the Moon: A reevaluation, Part I. In: *Lunar Planet. Sci. Conf. XXXII, Abstract No. 1658.* Lunar Planetary Institute, Houston (CD-ROM).

Norman, M.D., Bennett, V.C., Ryder, G., 2002. Targeting the impactors: siderophile element signatures of lunar impact melts from Serenitatis. *Earth Planet. Sci. Lett.* **202**, 217–228.

Nyquist, L.E., Shih, C.-Y., Reese, Y., Bogard, D.D., 2005. Age of lunar meteorite LAP 02205 and implications for impact-sampling of planetary surfaces. In *Lunar Planet. Sci. Conf. XXXV, Abstract No. 1374.* Lunar Planetary Institute, Houston (CD-ROM).

Papike, J.J., Hidges, F.N., Bence, A.E., Cameron, M., Rhodes, J.M., 1976. Mare basalts: crystal chemistry, mineralogy, and petrology. *Rev. Geophys. Space Phys.* **14**, 475–540.

Phinney, W.C., Morrison, D.A., 1990. Partition coefficients for calcic plagioclase: implications for Archean anorthosites. *Geochim. Cosmochim. Acta* **54**, 1639–1654.

Righter, K., Walker, R.J., Warren, P.H., 2000. Significance of highly siderophile elements and Os isotopes in the lunar and terrestrial mantles. In: Canup, R., Righter, K. (Eds.), *Origin of the Earth and Moon*. University of Arizona Press, Tucson, pp. 291–322.

Righter, K., Brandon, A.D., Norman, M.D., 2004. Mineralogy and petrology of unbrecciated lunar basaltic meteorite LAP 02205. In *Lunar Planet. Sci. Conf. XXXV, Abstract No. 1667*. Lunar Planetary Institute, Houston (CD-ROM).

Rhodes, J.M., Hubbard, N.J., 1973. Chemistry, classification, and petrogenesis of Apollo 15 mare-basalts. In: *Lunar Sci. Conf. IV*, Lunar Planetary Institute, Houston, pp. 1127–1148.

Rhodes, J.M., Blanchard, D.P., Dungan, M.A., Brannon, J.C., Rodgers, K.V., 1977. Chemistry of Apollo 12 mare-basalts: Magma types and fractionation processes. In: *Proc. Lunar Sci. Conf. VIII*, Lunar Planetary Institute, Houston, pp. 1305–1338.

Rutherford, M.J., Hess, P.C., Daniel, G.H., 1974. Experimental liquid line of descent and liquid immiscibility for basalt 70017. *Proc. Lunar Sci. Conf. V*, 569–583.

Ryder, G., 1985. Catalog of Apollo 15 rocks (three volumes). Curatorial Branch Pub. 72, JSC 20787.

Ryder, G., Schuraytz, B.C., 2001. Chemical variation of the large Apollo 15 olivine-normative mare-basalt rock samples. *J. Geophys. Res.* **106**, 1435–1451.

Sano, Y., Terada, K., Takeno, S., Taylor, L.A., McSween, H.Y., 2000. Ion microprobe uranium-thorium-lead dating of Shergotty phosphates. *Meteorit. Planet. Sci.* **35**, 341–346.

Sato, M., 1976. Oxygen fugacity and other thermochemical parameters of Apollo 17 high-Ti basalts and their implications on the reduction mechanism. *Proc. Lunar Sci. Conf. 7th*, 1323–1344.

Sato, M., Hickling, N.L., McLane, J.E., 1973. Oxygen fugacity values of Apollo 12, 14, and 15 lunar samples and reduced state of lunar magmas. *Proc. Lunar Sci. Conf. 4th*, 1061–1079.

Schnare, D.W., Taylor, L.A., Day, J.M.D., Patchen, A.D., 2005. Petrography and mineral characterization of lunar mare basalt meteorite LAP 02224. In: *Lunar Planet. Sci. Conf. XXXV, Abstract No. 1428.* Lunar Planetary Institute, Houston (CD-ROM).

Shafer J., Neal C. R. Castillo P., 2004. Compositional variability in lavas from the Ontong Java Plateau: results from basalt clasts within the volcaniclastic sequence of Ocean Drilling Program Leg 192 Site 1184. In: Fitton J.G., Mahoney J.J., Wallace P.J., Saunders A.D. (Eds.), *Origin and Evolution of the Ontong Java Plateau J. Geol. Soc. London Spec. Pub.* **229**, pp. 333–351.

Snyder, G.A., Taylor, L.A., 1992. Petrogenesis of the Western Highlands of the Moon: Evidence from a diverse group of whitlockite-rich rocks from the Fra Mauro Formation. *Proc. Lunar Planet. Sci., XXII*, Pergamon, New York, pp. 399–416.

Takeda, H., Arai, T., Saiki, K., 1993. Mineralogical studies of lunar meteorite Yamato-793169. In: *NIPR Symp. Antarct. Meteorites VI*, pp. 3–13.

Taylor, L.A., Day, J.M.D., 2005. FeNi metal grains in LaPaz Mare basalt meteorites and Apollo 12 Basalts. In: *Lunar Planet. Sci. Conf. XXXV,*

Abstract No. 1417. Lunar Planetary Institute, Houston (CD-ROM).Taylor, S.R. (1982) Planetary Science: A lunar perspective. Lunar & Planetary Institute, Houston, pp. 481.

Taylor, L.A., Misra, K.C. 1975. Pyroxene-phyric basalt 15075: petrography and petrogenesis. Proc. 6th Lunar Sci. Conf., *Geochim. Cosmochim. Acta,* Suppl. 6, 165–179.

Taylor, L.A., Kullerud, G., Bryan, W.B., 1971. Opaque mineralogy and textural features of Apollo 12 samples and a comparison with Apollo 11 rocks. In: *Lunar Planet. Sci. Conf.,* LPI, Houston, pp. 855–871.

Taylor, L.A., Uhlmann, D.R., Hopper, W., Misra, K.C., 1975. Absolute cooling rates of lunar rocks: theory and application. *Proc. 6th Lunar Sci. Conf., Geochim. Cosmochim. Acta* (Suppl. 6), 181–191.

Taylor, L.A., Patchen, A., Taylor, D.-H.S., Chambers, J.G., McKay, D.S., 1996. X-ray digital imaging petrography of lunar mare soils: modal analysis of minerals and glasses. *Icarus* **124**, 500–512.

Terada, K., Sano, Y., 2004. Ion microprobe U–Th–Pb dating and REE analyses of phosphates in the Nakhlites Lafayette and Yamato-000593/000749. *Meteorit. Planet. Sci.* **39**, 2033–2041.

Terada, K., Monde, T., Sano, Y., 2003. Ion microprobe U–Th–Pb dating of phosphates in Martian meteorite ALH 84001. *Meteorit. Planet. Sci.* **38**, 1697–1703.

Tuthill, R.L., Sato, M., 1970. Phase relations of a simulated lunar basalt as a function of oxygen fugacity ad their bearing on the petrogenesis of the Apollo 11 basalts. *Geochim. Cosmochim. Acta* **34**, 1293–1302.

Vetter, S.K., Shervais, J.W., Lindstrom, M.M., 1987. Petrology and geochemistry of olivine-normative and quartz-normative basalts from Regolith breccia 15498: New diversity in Apollo 15 mare basalts. In: *Lunar Planet. Sci. Conf. XVIII*, Lunar Planetary Institute, Houston, pp. 255-271.

Walter M. J., Newsom H. E., Ertel W., Holzheid A., 2000. Siderophile elements in the Earth and Moon: Metal/silicate partitioning and implications for core formation. In: Origin of the Earth and Moon, University of Arizona Press. pp. 265–289.

Warren, P.H., Kallemeyn, G.W., 1989. Elephant Moraine 87521: the first lunar meteorite composed of predominantly mare material. *Geochim. Cosmochim. Acta* **53**, 3323–3330.

Warren, P.H., Kallemeyn, G.W., 1991. Geochemical investigation of five lunar meteorites: implications for the composition, origin and evolution of the lunar crust. In: *NIPR Symp. Antarct. Meteorites IV*, Tokyo, Japan, pp. 91–117.

Warren, P.H., Kallemeyn, G.W., 1993. Geochemical investigation of two lunar meteorites: Yamato-793169 and Asuk-881757. Proc. NIPR Symp. Antarctic. *Meteorites.* **6**, 35–57.

Yanai, K., Kojima, H., 1991. Varieties of lunar meteorites recovered from Antarctica. In: *NIPR Symp. Antarct. Meteorites IV*, pp. 70–90.

Zinner, E., Crozaz, G., 1986a. A method for the quantitative measurement of rare earth elements in the ion microprobe. *Intl. J. Mass Spec. Ion. Proc.* **69**, 17–38.

Zinner, E., Crozaz. G. 1986b. Ion Probe Determination of the Abundances of All the Rare Earth Elements in Single Mineral Grains. *SIMS V*, pp. 444–446.